

A high-fiber diet mimics aging-related signatures of caloric restriction in mammals

Received: 14 October 2024

Accepted: 6 June 2025

Published online: 01 July 2025

Fangchao Hu^{1,2}, Lu Yu^{1,2}, Xingyu Tu^{1,2}, Rong Huang^{1,2}, Xinyue Yan¹,
Liping Wang¹, Yang Wei¹, Xinlin Wei¹✉ & Ziyun Wu¹✉

Caloric restriction (CR) delays aging-related hallmarks in various organisms by slowing growth and development while enhancing metabolic homeostasis. However, desirable diets that harness the metabolic benefits of CR without imposing food intake restrictions remain elusive. Here we evaluated the effects of a high-fiber diet we developed, in which 30% of the macronutrients in a standard diet are replaced with indigestible cellulose, compared to a CR control consisting of a nighttime-2h-restricted feeding regimen. Our findings show that the 2h-restricted feeding triggered a robust systemic response associated with the anti-aging benefits typically observed with CR. Intriguingly, the high-fiber diet did not reduce food intake but mimicked the aging-related signatures of CR in male mice from young to old age. These results indicate that the high-fiber diet confers promising benefits for metabolic homeostasis and represents a valuable candidate for further health and aging studies.

Caloric restriction (CR), the reduction of food intake without malnutrition, has become a gold standard in anti-aging studies¹. Despite the development and application of various CR-like protocols, such as ketogenic diets (KDs), intermittent fasting (IF), fasting-mimicking diets (FMDs), time-restricted feeding (TRF), protein restriction (PR), and methionine restriction (MR), many of these approaches involve excessive fasting and may lead to impaired growth, development, and other adverse effects^{2,3}. A desirable caloric restriction mimetic (CRM) should emulate the growth and development seen with ad libitum feeding, while reproducing the metabolic, hormonal, and physiological benefits of CR without the drawbacks of excessive fasting and other undesirable side effects^{4,5}. Additionally, a CRM should improve aging-related hallmarks, confer protection against a variety of stressors, and produce CR-like effects on aging and age-related diseases⁶.

Unfortunately, discovering an ideal CRM remains a formidable challenge^{2,3,6,7}. Rapamycin, a Food and Drug Administration (FDA)-approved natural compound, has been proposed as a preeminent CRM candidate. It robustly extends lifespan robustly in many model organisms, including various mice models, even when initiated in 20-month-old wild-type mice⁸. However, despite the considerable attention that rapamycin and other mechanistic target of rapamycin complex 1 (mTORC1) inhibitors have garnered in the anti-aging

community, their potential side effects, such as immunosuppression, hyperlipidemia, and hyperglycemia, must be carefully evaluated in clinical trials^{9,10}. On the other hand, accumulating evidence suggest that the type and ratio of macronutrients in the diet, including carbohydrates, fats and proteins, exert a profound effect on growth, metabolism and longevity in model organisms, ranging from yeast to mice^{2,11,12}. Moreover, some of these anti-aging dietary interventions do not necessarily involve reducing calorie or overall food consumption. Thus, it is conceivable that a desirable dietary CRM with fewer safety-related concerns commonly associated with drug development could be developed. However, it is worth noting that very few non-CR diet related longevity studies have included a classic CR as a positive control to parallelly evaluate CR-like benefits on growth, development, metabolism, and longevity³.

Dietary fibers are not hydrolyzed by endogenous enzymes in the small intestine but are partially or totally fermented by gut microbiota in the large intestine¹³. High-fiber diet consumption is typically linked to various health benefits, such as weight control, hunger reduction and satiety prolongation^{14,15}. In this context, we hypothesize that partially replacing macronutrients with dietary fibers may replicate CR-like benefits without unwarranted fasting and weight loss. To evaluate the hypothesis, we investigated the growth, food intake, transcriptome

¹Department of Food Science and Engineering, School of Agriculture and Biology, Shanghai Jiao Tong University, Shanghai, China. ²These authors contributed equally: Fangchao Hu, Lu Yu, Xingyu Tu, Rong Huang. ✉ e-mail: weixinlin@sjtu.edu.cn; wuziyun@sjtu.edu.cn

and metabolome in 3-month-old male C57BL/6J mice that were fed several high-fiber diets modified from the standard growth diet (AIN-93G). In one of these diets, 30% (w/w) of the components, primarily consisting of macronutrients, were substituted with cellulose, while vitamins and minerals were kept consistent. This dietary modification was found to have no significant impact on body weight over a two-week growth period. Furthermore, we found that this diet could induce a robust systemic response associated with the anti-aging benefits typically observed with CR, a phenomenon not observed in other high-fiber diets. Moreover, this high-fiber diet can help middle-aged and naturally aging mice improve glucose and lipid metabolism, reverse declines in motor abilities, and alleviate impairments in learning and memory function. Consequently, this diet emerges as a promising candidate for further evaluation of its CRM effects on health and aging.

Results

Effects of high-fiber diets on behavior and body weight in young male mice

To investigate the variance in dietary fibers for the substitution of macronutrients, we selected two representatives, inulin and cellulose, which are distinct due to their difference in physicochemical characteristics¹⁴. Inulin, a soluble and highly fermentable dietary fiber, has been extensively investigated and finds diverse applications in both food and medicine. In contrast, cellulose is insoluble, minimally fermentable, and a commonly employed fiber component in various mouse diet studies¹⁴. We redesigned the standard AIN-93G diet to obtain four different diets by replacing either corn starch or the entire macronutrients with the two selected fibers, thus the total fiber (including the original 5% cellulose) in the eight high-fiber diets range from 15% to 35% (Supplementary Fig. 1a). This range is commonly used in CR studies. Additionally, we implemented a nighttime 2 h ad libitum feeding and 22 h fasting protocol, serving as the CR positive control (Fig. 1a). Nighttime-restricted feeding has been shown to improve numerous health parameters more effectively than daytime-restricted feeding in mice^{16–19}. Notably, a nighttime-2 h 30% CR was reported to extend the lifespan of wild-type C57BL/6J mice by 35%, whereas non-time-restricted 30% CR only resulted in a 10% lifespan extension²⁰.

To test the palatability of these diets, 20 h fasted young adult (eight-week-old) male C57BL/6J mice were initiated on feeding (day 0) with the high-fiber diets. All groups, except for IF30m, showed a similar pattern of food consumption during the first 4 h (Fig. 1b and Supplementary Fig. 1b). IF30m might exhibit lower palatability than the other diets, as we observed that after the initial 1-h feeding, the mice consumed only 12% of the total food intake within 4-h period. Nevertheless, after two weeks of feeding (day 14), all groups displayed remarkably similar results, with food intake gradually decreased in the 4 h (Supplementary Fig. 1c). This aligns with findings from time-restricted feeding studies, where mice tend to consume food to the fullest extent when it becomes accessible^{18,20–22}. In addition, the mice consumed more in the first four days and then stabilized, indicating adaptation to all the diets (Fig. 1c, d). We then applied the average values from day 6 to 14 to evaluate the food intake. In the CR group, mice were allowed daily access to food for 2 h and consumed ~80% of the amount eaten by mice in the unrestricted feeding RD (regular diet) group within 24 h (Fig. 1e). Mice in CF30m group had the most food intake, which was 47% higher than the control RD group (Fig. 1e). Unlike food intake, the body weight of mice in all groups steadily gained over the course of the two weeks, as expected (Fig. 1f, g). Interestingly, the average weight in each group closely resembled that of the RD group, with the exception of the CR group, which exhibited a 17% reduction (Fig. 1h).

To further investigate whether a specific nutrient factor played a key role in body weight, we conducted an analysis of nutrient intake based on data derived from the diet composition and food intake

(Fig. 1i and Supplementary Fig. 1a). Firstly, animals in the CF30 group exhibited the highest protein intake, which was 39% higher compared to the RD group. In contrast, animals fed the CF30m diet showed protein intake similar to that of the RD group (Fig. 1j). This difference can be attributed to the CF30m diet's lower protein composition and higher consumption, while the CF30 diet maintained a similar protein proportion to the RD diet. Secondly, carbohydrate intake appears to be closely correlated to the corn starch ratios in the diets, given that starch is the major carbohydrate component in the diet (Fig. 1i, k). Thirdly, the CF30 group of mice presented the highest calorie intake, which was 13% higher, compared to the RD group (Fig. 1l and Supplementary Fig. 1m, n). By comparison, mice in the IF10 to IF30 groups had significantly lower calorie intake due to the lower energy density of their diets and reduced food consumption. Lastly, we observed that the inulin groups displayed a disconnect between food intake and water intake (Supplementary Fig. 1e–g). This suggests that both types of fiber-rich diets may contribute to reduced water intake, a phenomenon that warrants further investigation to determine the underlying reasons. However, mice in CR group exhibited higher water intake²³, with nearly half of their water consumption occurring within the 2-h feeding window. This is likely due to water intake can facilitate the speed of food consumption during the 2-h binge eating pattern^{18,20–22}.

Overall, our findings highlight the significant impact of this fiber replacement intervention on food intake, weight control, and nutrient optimization. As we observed, animals in the CF30m group consumed more food (+47%), but did not exhibit an increase in body weight (-2%), protein (+1%), calories (+1%) or carbohydrates (+1%). On the other hand, animals fed the CF30 diet consumed more protein (+39%), whereas their body weight did not increase (-5%) (Fig. 1e–l). In alignment with previous studies^{20,22}, our 2 h night CR protocol resulted in a 20% reduction in food intake, akin to a classical CR regimen in which mice were subjected to ~30% CR and consume their daily allotment within a ~2 h window as a single meal.

The night 2-hour feeding regimen mimics the transcriptional signatures of CR

To investigate the molecular-level effects of the high-fiber diets feeding, we conducted RNA sequencing (RNA-seq) analysis on mouse liver samples from six feeding groups (CR, RD, IF30, IF30m, CF30, CF30m). All 36 animals were sacrificed after a 4 h refeeding period on day 14 (Fig. 1b), and liver samples were collected within a 1 h window (from 10–11 p.m.) to minimize the influence of circadian rhythms on gene expression. We chose the 4 h timepoint after refeeding to profile mRNA expression because this duration is sufficient to induce significant changes in gene expression following refeeding. Additionally, this time window was selected to minimize the potential influence of the next meal, as this refeeding regimen aimed to mimic the human breakfast pattern.

To uncover the transcriptional signatures of nighttime 2 h ad libitum feeding, we performed differential gene expression analysis between the CR and RD mice (Supplementary Data 1). A total of 3663 genes were differentially expressed (FDR < 0.05) under CR versus RD (Fig. 2a). Of these, 2191 genes were down-regulated and 1472 were up-regulated. Strikingly, within the top downregulated transcripts ($-\log_{10}\text{FDR} > 5$ and $|\log_2\text{FC}| > 2$) were several major urinary proteins (*Mup11*, *Mup15*, *Mup16*, *Mup17*, *Mup18* and *Mup22*) and three cytochrome p450 enzymes (*Cyp4a10*, *Cyp4a14* and *Cyp4a59*) (Fig. 2a). The MUPs family consists of more than 20 isoforms, predominantly expressed in the liver, with significantly higher levels in males²⁴. They play a vital role in mate preference, social learning, and aggression^{25,26}. *Mup* genes have been reported to be influenced by both CR and high-calorie diets^{27,28}, suggesting their involvement in energy metabolism in the mouse liver. Gene ontology (GO) analysis revealed that the up-regulated genes were highly significantly related to energy metabolism,

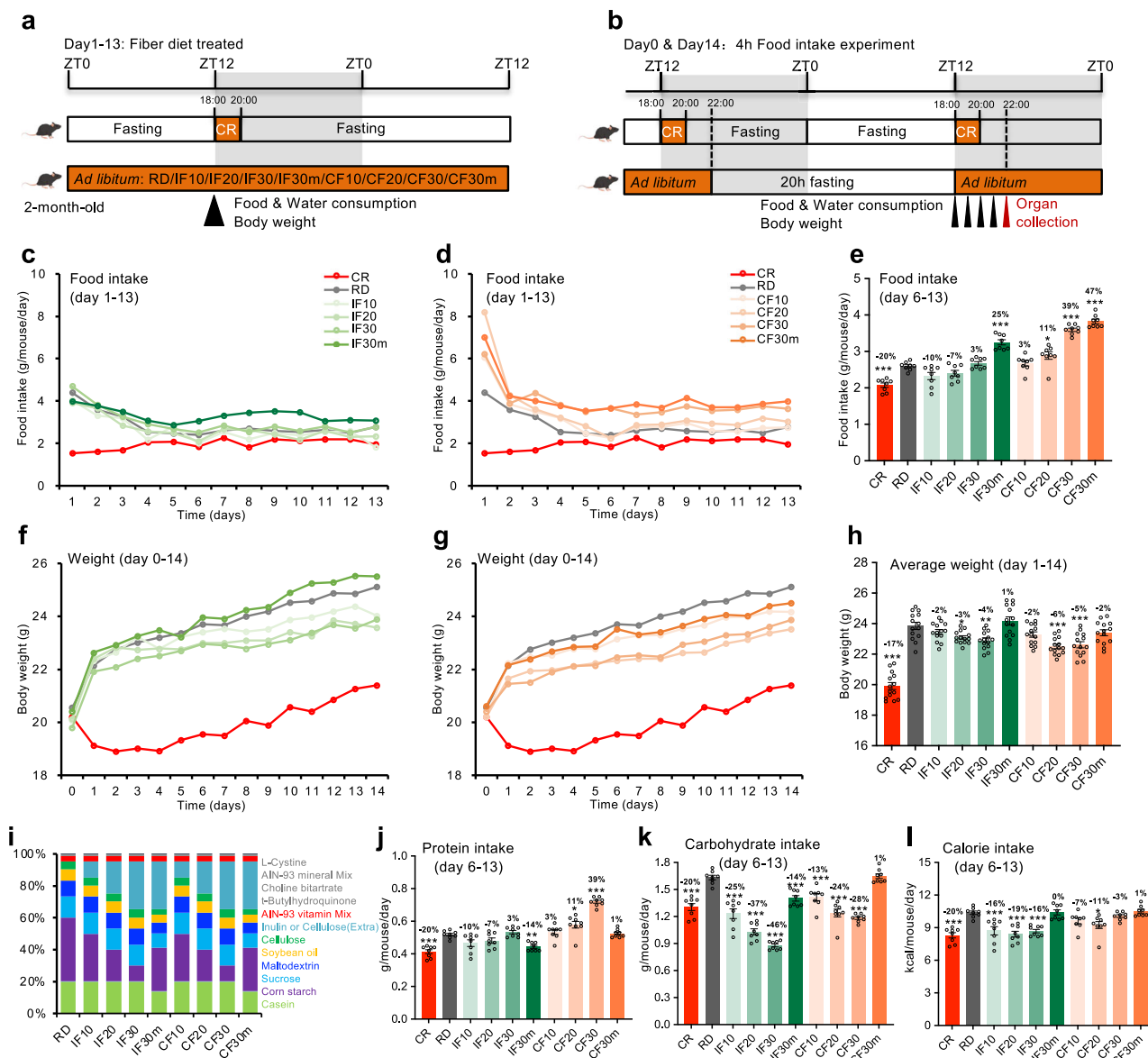


Fig. 1 | Effects of a fiber diet on physiological parameters in 2-month-old male mice. **a** Outline of feeding regimens (CR, RD, IF10, IF20, IF30, IF30m, CF10, CF20, CF30 and CF30m) during day 1 to 13. ZT: Zeitgeber Time, refers to the light exposure. Food and water consumption were measured at ZT12. **b** Experimental design showing the 4-h food intake test (except for the CR group) on day 0 and day 14. Food and water consumption were measured hourly. Trend in food intake for inulin (c) or cellulose (d) fiber diet groups from day 1 to 13. **e** Average food intake of all groups from day 6 to 13. Every point is the daily food intake of mice in each group from day 6 to day 13, a total of 8 points. Body weight of mice during the two-week

inulin (f) or cellulose (g) fiber diet intervention. **h** Average body weight of mice in all ten groups. Every point is the average body weight of mice in each group from day 1 to day 14, a total of 14 points. **i** Diet composition of eight redesigned fiber diets based on the AIN-93G formulation. Average protein (j), carbohydrate (k), or calorie intake (l) of mice from day 6 to 13. Every point is the average measurement data of 6 mice from day 6 to 13, a total of 8 points. Data are presented as mean \pm SEM, $n = 6$ mice per group. Statistical significance was determined by one-way ANOVA (Dunnett's test). * $P < 0.05$, ** $P < 0.01$, *** $P < 0.001$.

including lipid, carbohydrate, cholesterol metabolism and RNA splicing (Fig. 2b), whereas the downregulated genes were related to growth and development, including translation, ribosomal biogenesis, mitochondrial ATP synthesis (Fig. 2c). This is consistent with the existing understanding that CR hinders growth and development while promoting cytoprotective and metabolic activities to extend lifespan, which appears to be primarily achieved through the inhibition of mechanistic target of rapamycin (mTOR), insulin/insulin-like growth factor 1 (IGF-1) signaling pathways, along with the elevation of signaling pathways associated with Sirtuin1 (SIRT1) and AMP-activated protein kinase (AMPK)^{2,10,12,29}. Furthermore, the findings from KEGG pathway analysis mirrored the results obtained from the GO analysis (Supplementary Fig. 2a, b). However, it is noteworthy that the downregulated

genes were notably associated with various neurodegenerative diseases, which is particularly intriguing. This association can be attributed to the pivotal role played by ubiquitin-mediated proteolysis in the development of most neurodegenerative diseases³⁰.

To validate the transcriptional data obtained from our CR regimen, we reanalyzed RNA-seq data from a recent publication (Supplementary Data 2)²⁰. We utilized the same liver samples from wild-type C57BL/6J mice and implemented a similar 2 h nighttime feeding CR protocol. The overlap between CR/RD and CR-night-2h/AL groups consisted of 272 upregulated genes and 418 downregulated genes. GO analysis revealed that the upregulated genes were linked to extracellular matrix (ECM)³¹, collagen³¹, endoplasmic reticulum (ER)³², PI3K-Akt signaling pathway³³ (Fig. 2d), all of which have been previously

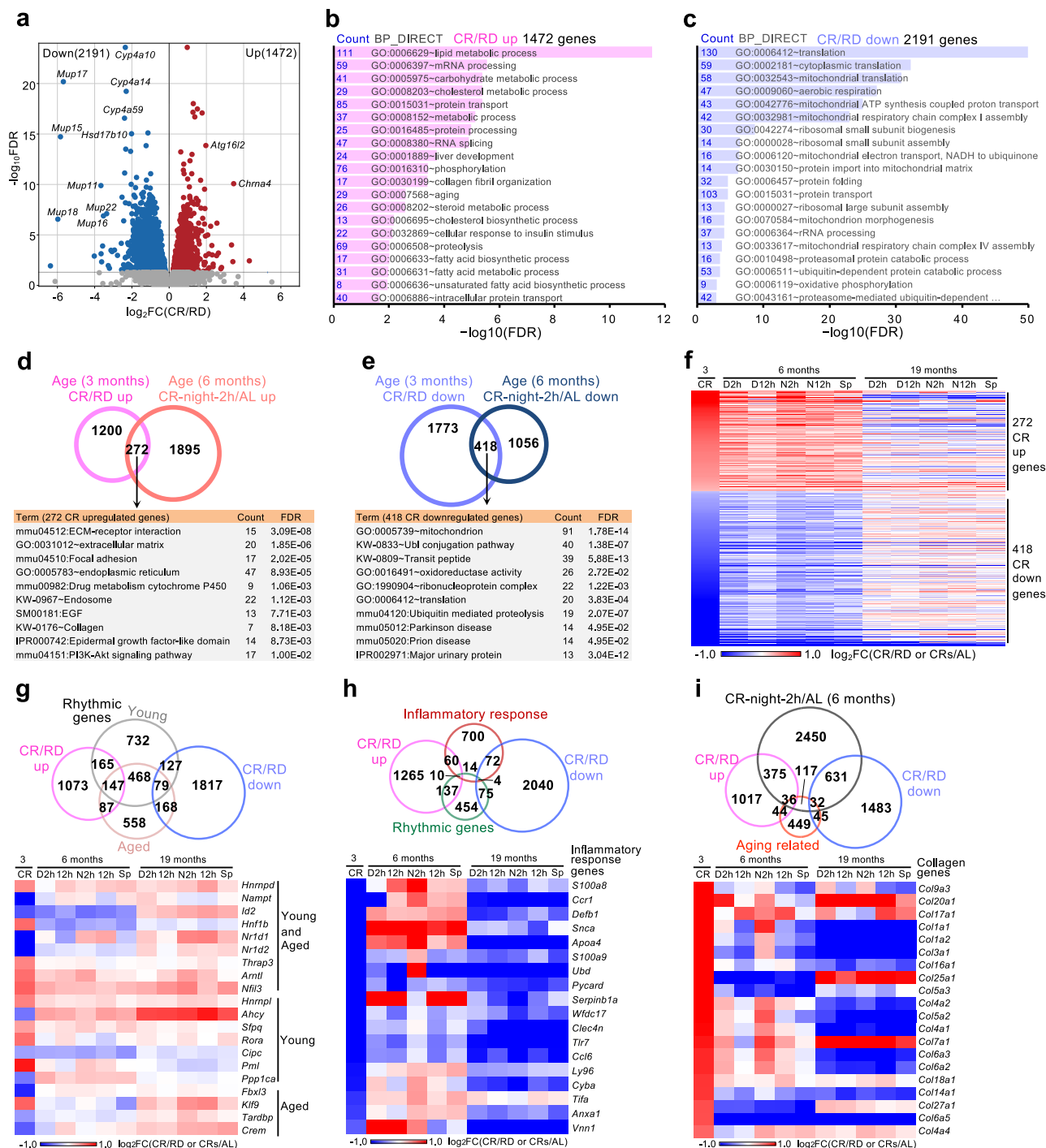


Fig. 2 | A night 2 h feeding regimen mimics the transcriptional patterns of CR in young male mice. a Volcano plots showing differentially expressed genes (DEGs) in liver of CR versus RD mice. Red denotes genes represent significantly upregulated genes in CR mice (1472 genes); blue denotes represent significantly downregulated genes in CR mice (2191 genes). DEGs were identified with FDR < 0.05. Top 20 GO terms enriched in genes upregulated (b) or downregulated (c) by CR. d Venn diagram (top) showing the overlap of CR/RD upregulated genes in 3-month-old mice (this study) with CR-night-2h/AL up-regulated genes in 6-month-old mice²⁰, and the pathway enrichment results of overlapping genes (bottom). e Venn diagram (top) showing the overlap of CR/RD downregulated genes in 3-month-old mice with CR-night-2h/AL downregulated genes in 6-month-old mice, and the pathway enrichment results of overlapping genes (bottom). f CR-mediated fold

change (FC) for overlapping genes across three age stages. g Venn diagram (top) showing the overlap between CR up/downregulated genes and rhythmic genes in young (6-month-old) or old (19-month-old) animals, heatmap (bottom) showing expression FC for the overlapping rhythmic genes across three age stages. The sets of rhythmic genes were identified from a previous study²⁰. h Venn diagram (top) showing the overlap among CR up/downregulated genes, rhythmic genes, and inflammatory response genes. Heatmap (bottom) showing expression FC for overlapping inflammatory response genes across three age stages. All Inflammatory response genes were from GO term inflammatory response (GO:0006954). i Venn diagram (top) showing the overlap among CR-regulated genes, aging related genes, and CR-night-2h/AL (6 months) DEGs. Heatmap (bottom) showing expression fold change (FC) for collagen genes across three age stages.

demonstrated to have expression patterns beneficial for longevity. On the other hand, the downregulated genes were associated to translation, ribosomal biogenesis, mitochondrion, MUPs and ubiquitin mediated proteolysis, as observed above (Fig. 2e). Furthermore, we conducted a comparison of the CR-mediated expression fold change (FC) for these overlapping genes across the three age stages, as illustrated in the heatmap (Fig. 2f). Evidently, a noticeable difference in the heatmap between the 6-month and 19-month, suggesting that CR exerts distinct effects on gene expression in young and old mice. This divergence is likely attributed to aging-related disease states and dysfunction within the aging organs. Notably, our CR-induced gene expression pattern (the first column, 3 months) exhibited a similar pattern to that observed in 6-month-old mice. Indeed, our downregulated genes under CR exhibited a higher degree of overlap with the downregulated genes in 6-month-old mice subjected to CRs, but conversely, an opposite pattern was noticed in 19-month-old mice (Supplementary Fig. 2c). This underscores the idea that the effects of CR can yield opposite outcomes in animals of different ages. Consequently, it highlights the need for careful consideration in the experimental design and interpretation of CR-related studies, particularly with regard to age-related variations³⁴.

Next, we examined the transcriptional expression of rhythmic genes, inflammatory response and other aging-related genes in our CR model. Firstly, a total of 773 genes (399 upregulated and 374 downregulated) in our CR model overlapped with the sets of rhythmic genes in either young or old animals (Supplementary Fig. 2d,g). This is consistent with our expectations, as many circadian cycling genes are known to be modulated by both CR and TRF^{20,35,36}. Secondly, 146 genes (70 upregulated and 76 downregulated) overlapped with the genes related to the inflammatory response (Fig. 2h). Interestingly, only 28 genes overlapped between the rhythmic and inflammatory response gene sets, suggesting that genes associated with inflammation may have a lower likelihood of being influenced by circadian rhythms. Moreover, CR seems to have a greater ability to suppress the expression of inflammatory genes in old mice compared to young mice, as evidenced by the noticeable difference between 6-month and 19-month mice in the heatmap (Fig. 2h and Supplementary Fig. 2d). This might be partially attributed to the fact that these genes are expressed at higher levels with aging and are very low in young animals, resulting in low enrichment in the differentially expressed gene (DEG) list in our CR model. Thirdly, our CR model significantly regulates 157 aging-associated genes (80 upregulated and 77 downregulated), which are involved in various pathways including TOR signaling, IIS signaling, collagen, heat shock proteins, glutathione S-transferase, autophagy, cytochrome P450, and UDP glucuronosyltransferase (Fig. 2i and Supplementary Fig. 2d). Notably, the mRNA expression of many (38/61) collagen genes was significantly elevated by our CR model, but this effect was partially attenuated in 6-month-old mice subjected to CR and further reduced in 19-month-old mice. This leads us to speculate that CR-induced enhancement of collagen-mediated extracellular matrix remodeling in young mice may partially contribute to the CR longevity³¹, as CR was found to be less effective when initiated later in life³⁷.

A high-fiber diet mimics the transcriptional signatures of CR in young male mice

The summary of transcriptomic results indicated that our nighttime 2-h feeding regimen can mimic the transcriptional signatures observed in the classic CR protocol. We then conducted a similar transcriptomic analysis on the high-fiber samples. Surprisingly, gene expression analysis revealed that only mice fed the CF30m diet presented a high number of DEGs (Fig. 3b, Supplementary Data 1). This similarity to CR was further confirmed by the heatmap, where CF30m showed a much closer resemblance to CR than the other groups (Fig. 3a). This alignment is substantiated by the significant correlation of gene expression

FC compared with RD for CR and CF30m groups (Fig. 3c). Once again, GO and KEGG pathway analyses yielded consistent results with those observed in our CR model (Fig. 3d, e and Supplementary Fig. 3a, b). Notably, many genes that were up-regulated by both CR and CF30m have been reported to have a lifespan-shortening effect when inhibited, suggesting their potential positive role in promoting longevity (Fig. 3f). In contrast, the down-regulated genes were linked to immune or inflammatory responses (Fig. 3g). Furthermore, these genes are associated with ribosome biogenesis, proteasome assembly, and the AMPK signaling pathway, all of which were significantly enriched in DEGs in both the CR and CF30m groups (Supplementary Fig. 3c–e).

The high-fiber diet has a more profound impact than CR in mice liver transcriptome

To determine the DEGs that were specifically regulated by CF30m, we conducted a comparative analysis of genes regulated by CR and CF30m compared with RD. As expected, more than half of the genes regulated by CR overlapped with those regulated by CF30m. Specifically, 853 genes were upregulated, and 1672 genes were downregulated, and these were shared by both CR and CF30m (Fig. 4a). We then categorized these genes into 10 groups (Supplementary Data 3), denoted as I to X (Fig. 4a). Groups I to IV represent the four sets of genes (CR upregulated, CR downregulated, CF30m upregulated, CF30m downregulated), while groups V to VIII consist of genes specifically regulated by these four sets. Groups IX and X comprise genes that are shared commonly between the two sets. To identify the biological processes (BPs) specifically associated with these ten groups, we selected GO terms that were significantly overrepresented in only one group and not in the other groups (Fig. 4b, c and Supplementary Fig. 4). The significantly enriched terms by CF30m upregulated genes (group III) included chemical homeostasis, positive organization, negative translation, steroid response, rhythmic process, insulin pathway, ER organization (Fig. 4b). Importantly, in the CF30m uniquely downregulated genes set (group VIII), we identified a surprising enrichment of numerous terms related to immune responses (group VIII) (Fig. 4c), which was not significantly enriched in both CR and CF30m downregulated gene sets (Figs. 2c, 3e).

The elevated expression of immune system processes and inflammation related genes with aging were identified in mouse liver²⁰. To determine if these genes were also present in our study, we conducted a comparison by examining aging-regulated genes (19 months versus 6 months) under AL feeding conditions and compared them with our ten gene sets (Fig. 4d). Remarkably, CF30m specifically downregulated gene set (group VIII) exhibited a higher degree of overlap with aging-upregulated genes compared to aging-downregulated genes. Additionally, this overlap was more pronounced under AL feeding conditions than under the various CR conditions. These findings suggest that CF30m specifically downregulated genes associated with aging-related immune processes. Subsequently, we performed a comparison of the expression FC mediated by CF30m specifically in genes across the three age stages, as illustrated in the heatmap (Fig. 4e, f). Obviously, CF30m exerted a profound impact on the expression of these genes, evident from the notably deeper colors in the heatmap when compared to other conditions. Furthermore, the Spearman correlation heatmaps also indicated that the expression trends of these genes, when influenced by CF30m, closely resembled those observed in mice subjected to CR in the old age stage, rather than in young mice.

Among the CF30m uniquely downregulated genes of note include allergic reactions protein high affinity IgE receptor (*Fcer1g*), interferon-gamma inducing proinflammatory cytokine factor interleukin 18 (*Il18*), immune response associated secretory leukocyte peptidase inhibitor (*Slpi*), immune reaction associated type III intermediate filament (IF) protein vimentin (*Vim*), C-X-C motif chemokine ligand 16 (*Cxcl16*), tumors-induced megakaryocyte potentiating factor (*Msln*), obesity-

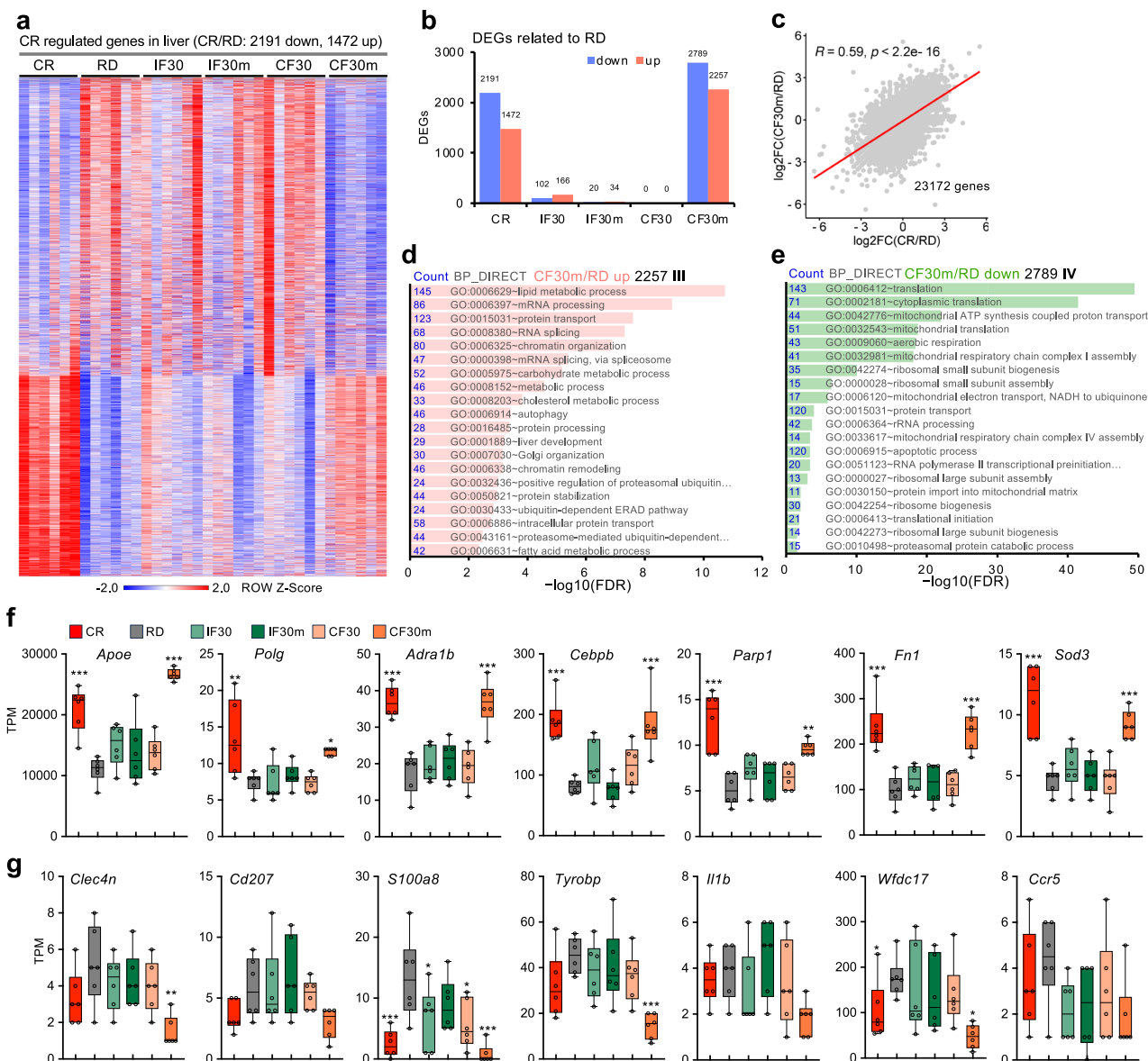


Fig. 3 | A high-fiber diet mimics the transcriptional patterns of CR in 2-month-old male mice. a Heatmap of CR-regulated genes in liver ($n = 6$ mice per group; $FDR < 0.05$). **b** Bar chart showing the number of DEGs across five feeding conditions compared to the RD group. **c** Spearman correlation plots showing significant correlation in gene expression FC between the CR and CF30m groups, compared to RD. **d** Top 20 GO terms enriched in genes upregulated (**d**) or downregulated (**e**) by CF30m. **f** Expression of representative lifespan-related genes known to shorten

lifespan when inhibited. Box-and-whisker plots (minimum, 25th percentile, median, 75th percentile, maximum), $n = 6$ biologically independent samples per group. **g** Expression of representative genes associated with immune or inflammatory responses. Box-and-whisker plots (minimum, 25th percentile, median, 75th percentile, maximum), $n = 6$ mice per group. Data are presented as mean \pm SEM, $n = 6$ mice per group. Statistical significance was determined by one-way ANOVA (Dunnett's test). * $P < 0.05$, ** $P < 0.01$, *** $P < 0.001$.

induced serine protease inhibitor A12 (*Serpina12*) (Fig. 4g). Among these CF30m specifically upregulated genes of note include cytoprotective factor heat shock protein 1B (*Hspa1b*), lipid metabolism-linked protein ATP-binding cassette sub-family A member 2 (*Abca2*), cell proliferation suppression factor poly(rC) binding protein 4 (*Pcbp4*), collagen synthesis enzyme prolyl 4-hydroxylase subunit alpha-2 (*P4ha2*), cytochrome p450 oxidoreductase (*Por*), glutathione homeostasis mediator gamma-glutamyltransferase 6 (*Ggt6*), inflammation-associated protein granulatin (*Grn*) (Fig. 4h).

The night 2 h feeding regimen mimics the metabolomic effects of CR in young mice

To determine whether the effect of our CR regimen on transcriptional alterations would also extend to metabolite level, corresponding to changes in gene expression, we identified a total of 296 downregulated

and 350 upregulated metabolites ($P < 0.05$ and $|FC| > 1.5$) under CR versus RD (Supplementary Fig. 5a and Supplementary Data 4). Not surprisingly, principal component analysis (PCA) clearly demonstrated that samples from both CR and CF30m groups clustered separately from the other groups (Supplementary Fig. 5b). Further GO analysis of these differentially abundant metabolites (DAMs) uncovered that the downregulated DAMs were significantly related to nucleotides metabolism (Supplementary Fig. 5c), whereas the upregulated DAMs were linked to lipid metabolism (Supplementary Fig. 5d). For example, among the downregulated metabolites included the nucleotides guanosine (G), deoxyadenosine (dA) and aminoimidazole carboxamide ribonucleotide (AICAR, also known as Z-nucleotide), the steroid dehydroepiandrosterone (DHEA, abundant hormone in the human body), and the HIV treatment drug efavirenz (benzoxazine) (Supplementary Fig. 5e); among the upregulated metabolites included the L-alpha-amino acids L-lysine

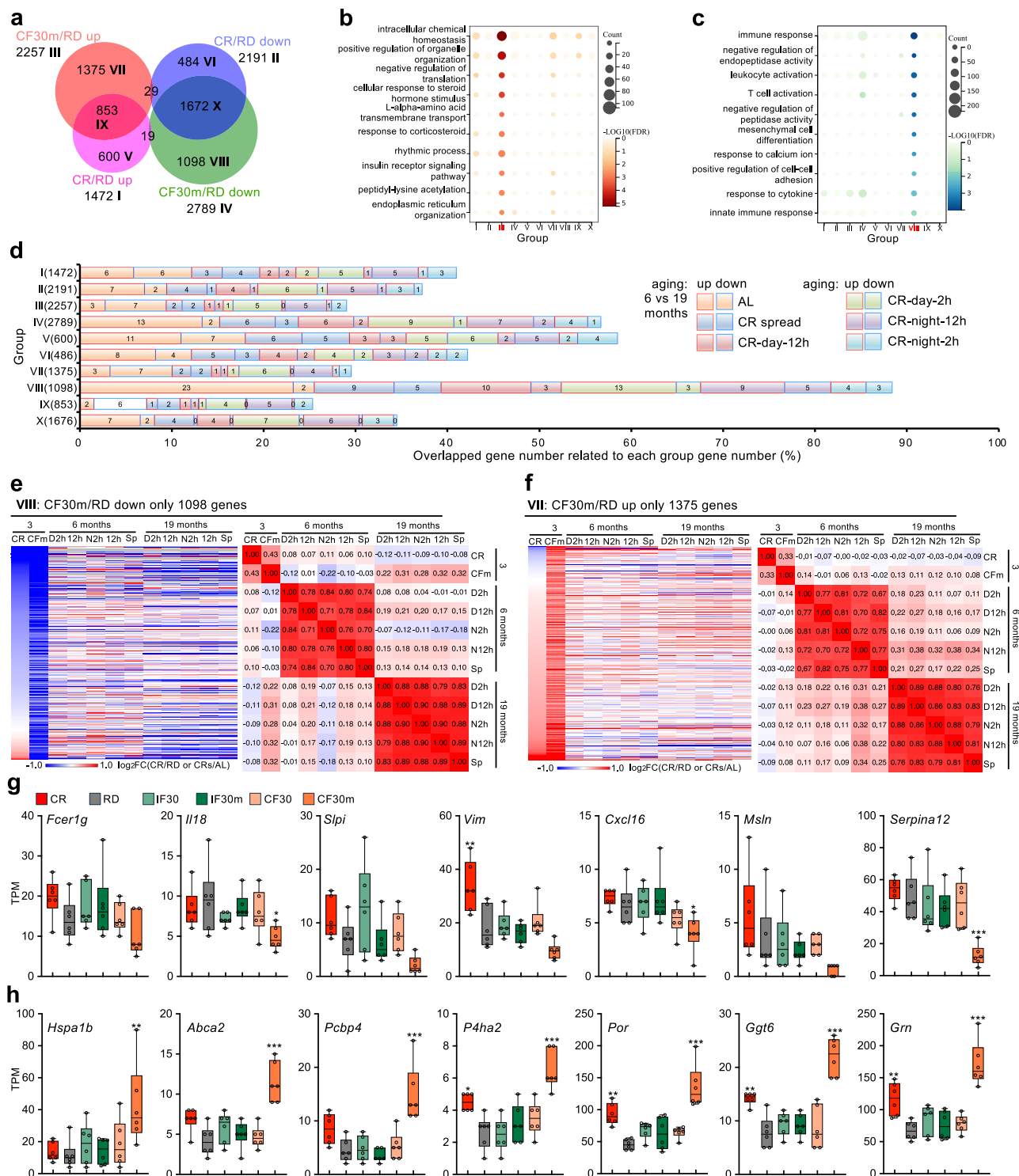


Fig. 4 | The high-fiber diet impacts the liver transcriptome more profoundly than CR in young male mice. a Venn diagram showing the overlap between CR/RD DEGs and CF30m/RD DEGs. The ten overlapping gene sets were numbered I to X (Supplementary Data S3). **b** Bubble chart showing GO terms significantly enriched in group III (CF30m upregulated genes) but not in other groups. **c** Bubble chart showing GO terms related to immune responses that were significantly enriched in group VIII (CF30m uniquely downregulated genes) but not in other groups. **d** Stacked bar chart depicting the percentage of overlapping genes between the ten gene sets and aging genes (19 months versus 6 months DEGs) across any CR condition. Red outlines represent aging upregulated genes; blue outlines represent aging downregulated genes. **e** Heatmap (left) showing expression FC for group VIII (CF30m uniquely downregulated genes) across three age stages. Gene expression matrix Spearman correlation heatmaps (right) showing

the similarity of expression pattern of group VIII (CF30m uniquely downregulated genes) under different feeding conditions. **f** Heatmap (left) showing expression FC for group VII (CF30m uniquely upregulated genes) across three age stages. Gene expression matrix Spearman correlation heatmaps (right) showing the similarity of expression pattern of group VII (CF30m uniquely upregulated genes) under different feeding conditions. **g** Expression of representative genes specifically downregulated by CF30m. Box-and-whisker plots (minimum, 25th percentile, median, 75th percentile, maximum), $n = 6$ mice per group. **h** Expression of representative genes specifically upregulated by CF30m. Box-and-whisker plots (minimum, 25th percentile, median, 75th percentile, maximum), $n = 6$ mice per group. Data are presented as mean \pm SEM, $n = 6$ mice per group. Statistical significance was determined by one-way ANOVA (Dunnett's test). * $P < 0.05$, ** $P < 0.01$, *** $P < 0.001$.

(low levels in patients with Parkinson's) and ornithine (associated with wound-healing effects and immune enhancement), the sulfinic acid hypotaurine (involved in taurine and hypotaurine metabolism), the glycerophospholipids LysoPC(18:3(6Z,9Z,12Z)) (anti-inflammatory properties) and PS(18:0/20:4(8Z,11Z,14Z,17Z)) (important for phospholipid biosynthesis) (Supplementary Fig. 5f). Information regarding these compounds was referenced from Human Metabolome Database (HMDB version 5.0)³⁸. Moreover, we carried out an integrated pathway over-representation analysis of our transcriptomic and metabolomic data³⁹. Indeed, the enriched GO terms observed in either the CR-regulated genes or the metabolite sets were also differentially enriched through joint analysis ($P < 0.05$), indicating a strong correlation between gene expression and metabolite level (Supplementary Fig. 5g, h).

The high-fiber diet alters the liver metabolome more profoundly than CR in young mice

We next conducted a metabolomic assessment of samples from the high-fiber diet groups to investigate whether CF30m had a more pronounced impact on the liver metabolome compared to CR, a trend similar to what we observed in the transcriptomic data. In contrast to the RNA-seq data, all experimental groups displayed several hundred DAMs relative to RD group (Fig. 5a and Supplementary Data 4). Interestingly, animals fed the four high-fiber diets showed a higher number of upregulated DAMs for reasons that remain unclear, although this was not observed for downregulated DAMs. A heatmap illustrating the relative abundance of CR-mediated DAMs revealed that the abundance of CR-downregulated metabolites was distinct from the other groups, while there was a similarity between CR and CF30m groups for their upregulated metabolites (Fig. 5b). This observation is consistent with the PCA results (Supplementary Fig. 5b), which suggested that CR and CF30m are separated. Consistently, 36% (127/350) of CR-upregulated metabolites were also elevated by CF30m, a proportion much higher than the overlap observed between the other groups (Fig. 6c).

Next, we conducted GO analysis of DAMs regulated by CF30m and CR. In brief, CF30m appeared to have a lesser impact on decreasing nucleotide metabolism compared to CR (Fig. 5d), but it had a more significant influence on increasing lipid metabolism (Fig. 5e). These findings were consistent with the results of gene expression and were confirmed by the joint analysis of DEGs and DAMs (Fig. 5f). Once again, many important metabolites were significantly regulated by CF30m but not by CR. Noteworthy downregulated metabolites were the sugar alcohol galactitol (a metabotoxin, neurotoxin, and hepatotoxin), the indole indoleacetic acid (IAA, a uremic toxin), the benzene phenylpyruvic acid (found at high levels in individuals with phenylketonuria), the nucleotide deoxyinosine monophosphate (dIMP) and the keto acid 3-oxododecanoic acid (Fig. 5g). Remarkable upregulated metabolites were the steroid estrone (a major mammalian estrogen), the omega-6 fatty acids linoleic acid (one of two essential fatty acids for humans) and eicosadienoic acid (a di-unsaturated fatty acid), the fatty acyl diacylglycerol (DAG) DG(18:1(11Z)/18:3(9Z,12Z,15Z)/0:0), and the prenil lipid gamma-tocotrienol (a derivative of vitamin E) (Fig. 5h)³⁸.

Most notably, we identified 192 lipids and lipid-like compounds among the 571 CF30m upregulated DAMs (Supplementary Data 4), including 66 fatty acyls (related to the structure and function of cell membranes), 51 glycerophospholipids (found in the lipid bilayer of cells), 31 steroids and steroids (hormones and signaling molecules), 30 prenil lipids (acting as antioxidants and contributing to vitamins A, E, and K), and 11 glycerolipids (involved in energy storage)⁴⁰. Interestingly, these lipids exhibited the highest concentration in the CF30m samples and the lowest concentration in the RD samples (Fig. 5i), demonstrating a more profound effect on lipid metabolism compared to CR, although other upregulated metabolites influenced by CF30m were not extensively investigated.

Short-chain fatty acids (SCFAs) are key metabolites produced predominantly in the colon through bacterial fermentation of

indigestible fibers by the gut microbiota⁴¹. These intestinally derived SCFAs have been implicated in numerous beneficial effects on energy metabolism, inflammation and immunity⁴². Therefore, SCFAs may represent a potential effector molecule underlying the health benefits of the CF30m diet. However, in contrast to the 192 lipid compounds analyzed, we found that both CR and CF30m exert limited effects on SCFA levels in the blood and liver of mice (Supplementary Fig. 6a,b). Additionally, ketone bodies are important lipid-derived molecules that serve as circulating energy sources during fasting and CR⁴³. To assess whether CF30m diet influences ketone body production, we measured blood levels of beta-hydroxybutyrate at 18:00 (following 22 h of fasting under CR) and 22:00 (after refeeding under CR). Consistent with previous findings⁴⁴, beta-hydroxybutyrate levels in CR mice increased after fasting but returned to baseline levels post-feeding. In contrast, the blood ketone levels in the RD and CF30m groups remained comparable (Supplementary Fig. 6c). These findings suggest that neither SCFAs nor ketone bodies are likely to serve as the primary effector molecules mediating the health benefits of the CF30m diet.

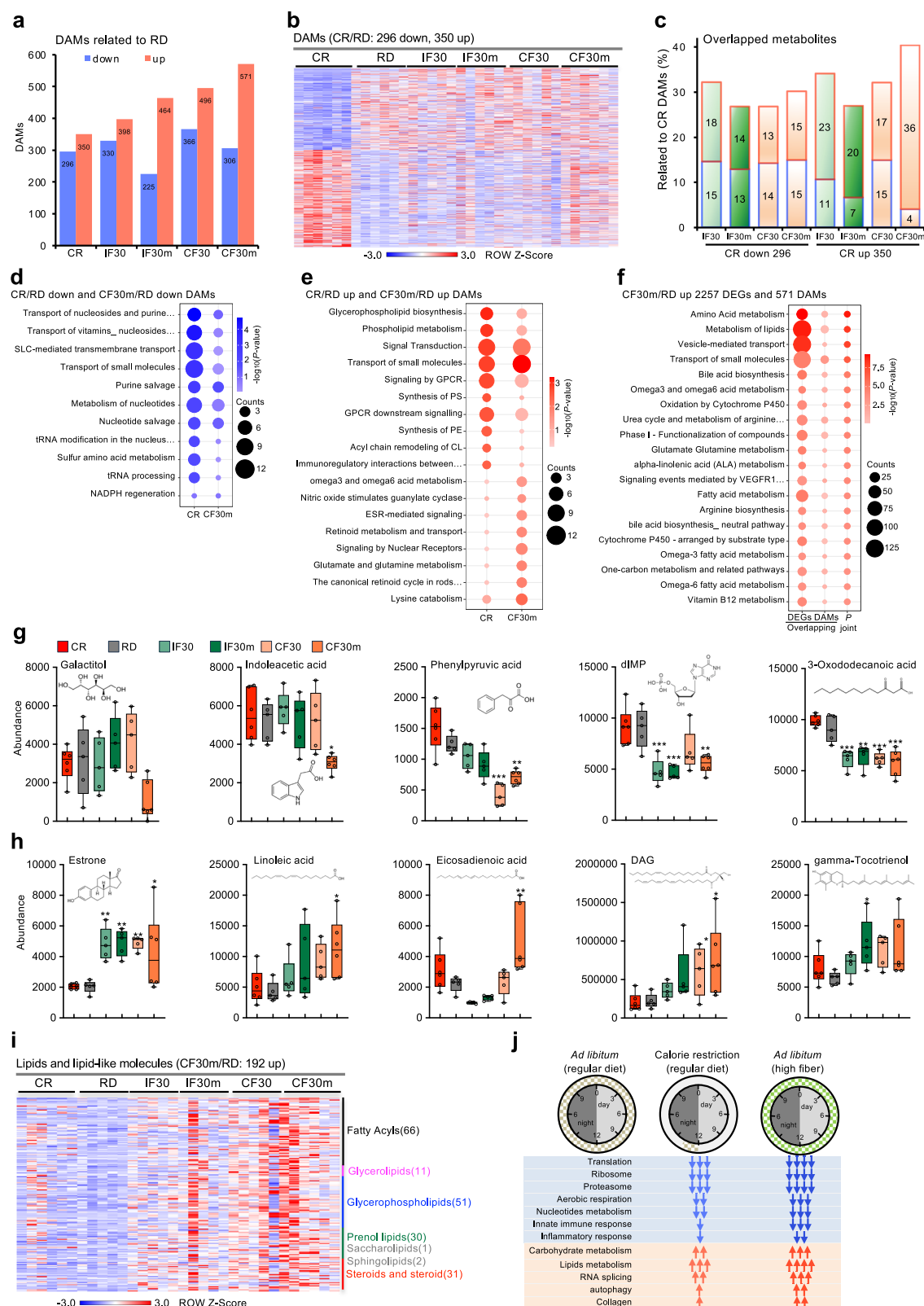
Collectively, our data suggest that the CF30m diet elicits a robust systemic response associated with longevity benefits typically observed with CR in young mice, this entails a downregulation of innate immunity, inflammation, and translation, coupled with an upregulation of lipid metabolism, collagen production, and autophagy (Fig. 5j).

A long-term high-fiber diet reverses aging-related signatures in middle-aged mice

To further evaluate the anti-aging effects of the high-fiber diet, six-month-old mice were fed either the AIN-93G diet or the CF30m diet for 4 months, until they reached middle age at 10 months (Fig. 6a). Over the 4-month period, food and water intake in both RD and CF30m groups remained relatively stable, with minor fluctuations (Fig. 6b and Supplementary Fig. 7a). Mice in CF30m group consumed more food (+34%) compared to those in RD group (Fig. 6c). Although calorie intake was similar between RD and CF30m groups (Supplementary Fig. 7b, c), CF30m group had a lower body weight (-6%) than RD group (Fig. 6d and Supplementary Fig. 7d). Thus, the high-fiber diet resulted in more food intake without altering overall energy intake, a pattern also observed in young mice.

Impaired glucose metabolism, reduced motor function, and cognitive decline are key indicators of aging⁴⁵. To further investigate, three-month-old young mice (Y3m group) were included as controls. In an oral glucose tolerance test, CF30m-fed mice displayed significantly lower blood glucose levels within 30 min of glucose administration, which were even slightly lower than those of the Y3m group (Fig. 6e, f). As expected, aging significantly reduced grip strength in the RD group compared to the Y3m group (Fig. 6g). However, the high-fiber diet noticeably improved grip strength in the CF30m group. Additionally, in the rotating rod test, CF30m-fed mice exhibited latency times and movement distances comparable to those of the Y3m group, which were higher than those of the RD group (Fig. 6h, i). This indicates that the high-fiber diet effectively mitigated age-related motor impairments. Furthermore, graying of fur, a prominent sign of aging in mice⁴⁶, was significantly reduced in the CF30m group compared to the RD group (Fig. 6j, k).

To assess cognitive functions, Y-maze test and Morris water maze tests were performed. Aging reduced the accuracy in the Y-maze, while the high-fiber diet improved accuracy compared to the RD group (Supplementary Fig. 7e). During the Morris water training period from day 1 to 5, middle-aged RD-fed mice exhibited no significant improvement in escape latency, which remained around 35 s (Fig. 6l). In contrast, CF30m-fed mice showed a marked reduction in escape latency, decreasing to about half of the initial latency by day 5, significantly outperforming the RD group (Fig. 6l). On day 6, after the platform was removed, CF30m-fed mice demonstrated



significantly higher target crossing counts than the RD group (Fig. 6m). Additionally, CF30m-fed mice spent more time in the target area and target quadrant than RD-fed mice (Fig. 6n, o). Interestingly, the high-fiber diet also reversed aging-associated changes in skin tissue. CF30m-fed mice exhibited significantly reduced subdermal thickness, resembling that of young mice, whereas aging increased subdermal thickness and reduced dermal thickness in RD-

fed mice (Fig. 6p, q). These findings align with previous studies showing aging-related dermal changes⁴⁷.

Transcriptomic analysis of liver tissues further highlighted the anti-aging effects of the high-fiber diet (Supplementary Data 5). PCA revealed distinct transcriptomic profiles between young (Y3m) and middle-aged (RD-fed) mice, with the CF30m diet shifting the transcriptome of middle-aged mice closer to that of young mice

Fig. 5 | Hepatic multi-omics profiles indicate a more significant alteration by the high-fiber diet in young mice. **a** Comparison of DAMs related to RD in the CR and four fiber groups. **b** Heatmap showing the abundance of CR-regulated DAMs across all high-fiber groups. Five to six biological replicates were performed for each condition. **c** Percentage overlap of DAMs between the four high-fiber groups relative to RD and CR relative to RD. Red borders indicate upregulated overlaps and blue borders indicate downregulated overlaps. **d** Representative GO terms and pathways enriched in DAMs downregulated by CR/RD and CF30m/RD. **e** Representative GO terms and pathways enriched in DAMs upregulated CR/RD up and CF30m/RD. **f** Top 20 pathways identified by joint pathway analysis using enrichment. These pathways were obtained by analyzing the overlap of 2257 DEGs and 571 DAMs upregulated by CF30m/RD. **g** Abundance of representative metabolites downregulated by CF30m. Box-and-whisker plots (minimum, 25th

percentile, median, 75th percentile, maximum). For CR and CF30m group, $n = 6$ mice; For RD, IF30, IF30m and CF30 group, $n = 5$ mice. **h** Abundance of representative metabolites upregulated by CF30m. Box-and-whisker plots (minimum, 25th percentile, median, 75th percentile, maximum). For CR and CF30m group, $n = 6$ mice; For RD, IF30, IF30m and CF30 group, $n = 5$ mice. **i** Heatmap showing classes of 192 lipid and lipid-like related compounds upregulated by CF30m. **j** Schematic comparison of hepatic transcriptomic and metabolomic signatures in C57BL/6J male mice under CR and CF30m feeding regimens. Arrows represent upregulated or downregulated genes; the quantity of arrows indicates the number of genes, while arrow color intensity reflects the level of gene expression. Data are presented as mean \pm SEM. Statistical significance was determined by one-way ANOVA (Dunnett's test). * $P < 0.05$, ** $P < 0.01$, *** $P < 0.001$.

(Supplementary Fig. 7f). Aging under RD conditions resulted in 977 DEGs, including 487 upregulated and 490 downregulated genes (Supplementary Fig. 7g). GO analysis indicated that aging upregulated genes associated with the unfolded protein response (Supplementary Fig. 7h), a hallmark of ER stress and a key manifestation of aging^{48,49}. Downregulated genes were primarily linked to fatty acid beta-oxidation, bile acid metabolism, and innate immune response (Supplementary Fig. 7i), including genes such as *Scd27a2*, *Acot3*, and *Cyp4a10* (Supplementary Fig. 7K). Remarkably, the number of DEGs in the CF30m group was only 30% of that in the RD group (Supplementary Fig. 7j), with many aging-related genes either restored or silenced in CF30m-fed mice. This strongly supports the ability of the high-fiber diet to rescue aging-related transcriptomic changes in middle-aged mice. Collectively, these findings demonstrate that a long-term high-fiber diet during adulthood effectively prevents aging-associated metabolic impairments, including impaired glucose metabolism and weakened lipid metabolism, while also preserving motor function, cognitive abilities, and skin integrity.

High-fiber diet mimics the healthy aging effects of CR in naturally aging mice

To investigate whether the high-fiber diet can resist aging, we used naturally aging mice (18 months) for dietary intervention. High-fat (HF) diet can cause metabolic problems such as obesity, blood sugar dysregulation and increased cholesterol levels, leading to decreased survival⁵⁰. Additionally, maternal HF diet induces long-term cognitive deficits that span across several generations⁵¹. Therefore, we used the high-fat diet as a control for promoting aging, while the anti-aging effect of CR, widely recognized, was used as a positive control to analyze the effect of the high-fiber diet on aging. Eighteen-month-old mice were fed RD, HF, and CF30m diets or subjected to CR for 4 weeks (Fig. 7a).

The food intake and water intake in each group closely resembled that of RD group (Fig. 7b and Supplementary Fig. 8a). As expected, caloric intake of the HF group was 21% higher, compared to RD group, while caloric intake of CF30m group was 14% lower (Supplementary Fig. 8b,c). Although the body weight of mice in RD group was relatively stable, HF diet caused the mice to gain 25% of their body weight, whereas CR and CF30m diet caused the mice to lose weight (Fig. 7c and Supplementary Fig. 8d). In the fourth week (19 months), mice on HF diet showed elevated blood glucose levels, while CR and CF30m groups had lower blood glucose levels than the RD group (Fig. 7d). The AUC of CR and CF30m groups was similar and lower than that of the HF group (Fig. 7e).

The increase in fat content and decline in lean mass are important signs of aging⁵². The HF group exhibited higher body fat content and lower lean mass compared to the RD group, while the CR and CF30m groups demonstrated the opposite trend (Fig. 7f and Supplementary Fig. 8e). Furthermore, mice in the CF30m and CR groups showed greater grip strength, and longer latency time and distance in the

rotating rod test compared to the RD group. In contrast, HF group impaired the motor abilities of the mice (Fig. 7g–i).

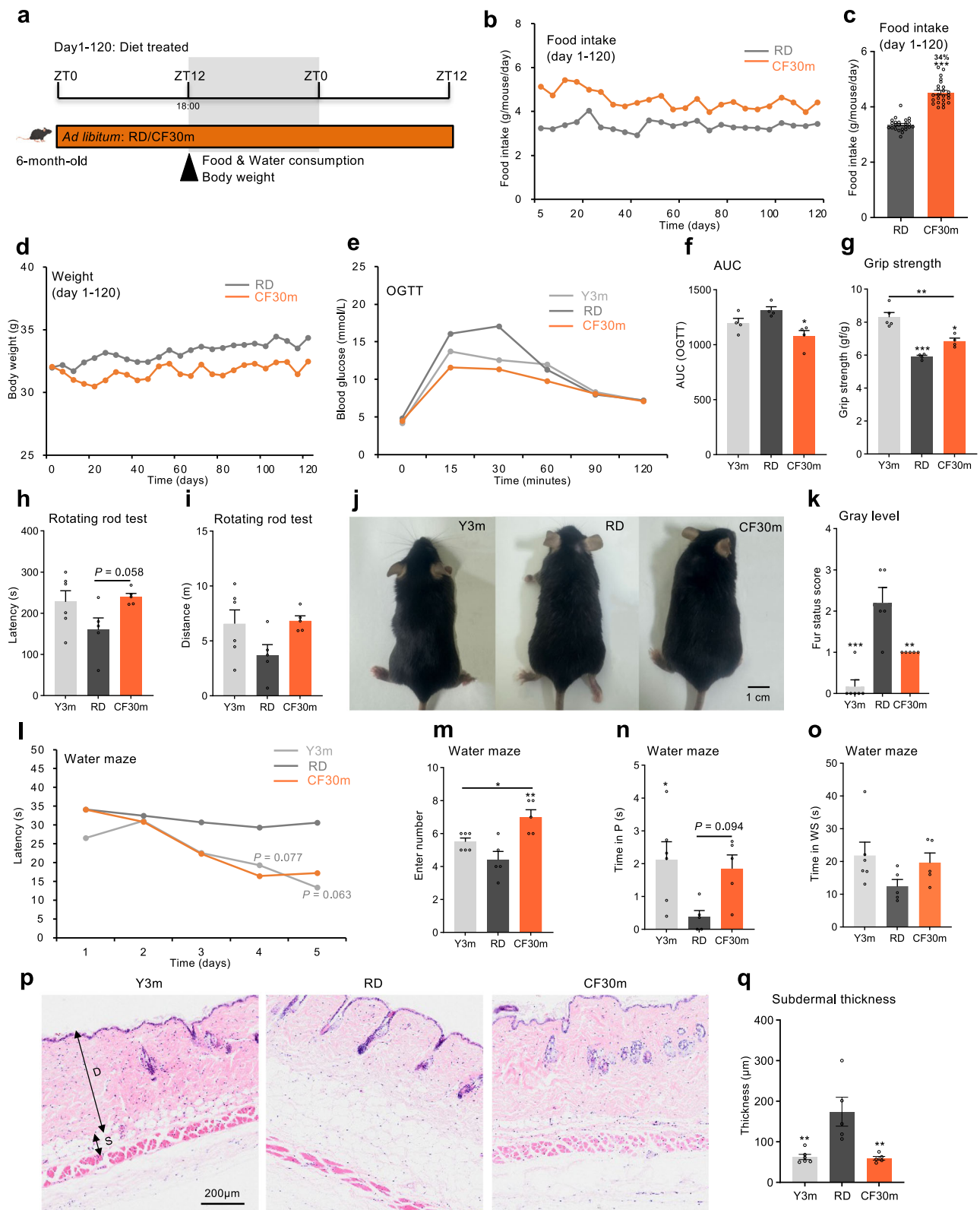
In the Morris water maze test, the CR and CF30m groups displayed superior learning and memory functions compared to the RD and HF groups during the training phase (day 1 to 5) (Fig. 7j). By day 5, the escape latency of the CF30m and CR groups was shorter than that of the RD group, with CF30m outperforming CR. On day 6, after removing the platform, the HF group struggled to locate the target area, while the CR and CF30m groups had more target crossings than the RD group (Fig. 7k). Furthermore, the CR and CF30m groups spent more time in the target area (Fig. 7l,m). These findings suggest that the high-fiber diet and CR could improve motor functions and cognitive abilities in aged mice.

Histological analysis of epididymal fat revealed a significant increase in the average adipocyte cross-sectional area in HF-fed mice compared to RD-fed mice, while CF30m- and CR-fed mice exhibited smaller adipocyte areas than RD-fed mice (Fig. 7n,o). In liver sections stained with H&E, RD-fed mice displayed prominent lipid droplets, infiltration of inflammatory cells, and hepatocellular edema. In contrast, CF30m- and CR-fed mice showed minimal lipid droplets and inflammatory cell infiltration, whereas HF-fed mice had an increased number of lipid droplets. However, hepatocellular edema was observed across all groups and was not alleviated by any of the dietary interventions.

We next analyzed the liver transcriptome. PCA revealed that the CR and CF30m groups clustered closely together and were distinctly separated from the HF and RD groups (Supplementary Fig. 8f). A total of 1643 genes were differentially expressed when comparing the CR and CF30m groups to the RD group (Supplementary Data 6). Correlation analysis further demonstrated a high degree of similarity between the CF30m and CR groups ($R = 0.95$). GO analysis showed that genes upregulated by the high-fat diet were predominantly associated with immune system processes and inflammation, while downregulated genes were linked to lipid metabolism (Supplementary Fig. 8h). This aligns with previous studies highlighting increased inflammation and reduced lipid metabolism as key hallmarks of aging²⁰. However, genes involved in lipid metabolism and innate immune response were either upregulated or downregulated by CR and CF30m in aged mice (Supplementary Fig. 8i,j). This dysregulation pattern, which was absent in young and middle-aged mice, further supports the notion that aging may induce an opposite expression trend⁵³. In summary, these findings suggest that, akin to CR, the CF30m diet administered during aging can enhance aging-related parameters, including improved glucose metabolism, reduced body fat, and enhanced motor function and cognitive performance in aged mice.

Discussion

CR is a highly challenging practice, and discovering a dietary mimic would offer significant advantages for adherence while also providing



valuable insights into the mechanisms behind CR. Diet quality and timing are crucial mediators of metabolism and healthy aging⁵. In this study, we considered both diet quality and feeding timing. Most notably, we devised a high-fiber diet modification based on the standard AIN-93G diet. This modification elicited a more pronounced CR-like effect on transcriptomic and metabolomic profiles in young mice liver, all while avoiding restrictions on food, calories, protein or carbohydrate intake, and without loss in body weight from young to aged

mice. Similar to CR animals, replacing 30% of macronutrients with indigestible cellulose while maintaining consistency in other nutrients reversed increases in body fat, reduced glucose tolerance, and improved motor abilities and cognitive functions in both middle-aged (10-month-old) and aged (19-month-old) mice.

In a previous study²¹, a 50% cellulose dilution of a purified diet resulted in ~30% reduction in caloric intake, significant reductions in body weight, fat mass, lean mass, and a shortened lifespan in 4-month-

Fig. 6 | Long-term high-fiber diet improves physical performance in middle-age mice. **a** Outline of feeding regimens (RD and CF30m) during day 1 to 120. Food and water consumption were measured at ZT12. Daily **(b)** and average **(c)** food intake for RD and CF30m groups over 120 days. For **c**, every point is the average food intake for every 5 days, 24 points in total. **d** Body weight changes during the four months. **e** Blood glucose levels after oral glucose gavage over a 120 min period. **f** Area under the curve (AUC) of glucose levels during the 120 min OGTT. $n = 4$ mice per group. **g** Grip strength comparison of Y3m, RD, and CF30m mice. $n = 4$ mice per group. **h, i** The latency time **(g)** and movement distance **(h)** in rotating rod test. For Y3m group, $n = 6$ mice; For RD and CF30m group, $n = 5$ mice. **j** Representative pictures of Y3m, RD and CF30m mice. For Y3m group, $n = 6$ mice; For RD and

CF30m group, $n = 5$ mice. **k** Fur status quantification using evaluation score (0–3, where 0 indicates no gray fur and 3 indicates substantial gray fur). For Y3m group, $n = 6$ mice; For RD and CF30m group, $n = 5$ mice. **l** Escape latency in the Morris water maze test. **m–o** Morris water maze measures: target platform enter number **(m)**, crossing time **(n)**, and WS quadrant crossing time **(o)**. For Y3m group, $n = 6$ mice. For RD and CF30m group, $n = 5$ mice; H&E-stained skin sections **(p)** and subdermal thickness quantification **(q)**. D, dermis; S, subdermis. For Y3m group, $n = 6$ mice; For RD and CF30m group, $n = 5$ mice. Data are presented as mean \pm SEM. Statistical significance was determined by one-way ANOVA (Tukey post-hoc test). * $P < 0.05$, ** $P < 0.01$, *** $P < 0.001$.

old C57BL/6J male mice. However, the same 50% cellulose dilution to the entire diet was observed to increase food intake (+75%), reduce body weight (-12.5%) and caloric intake (-28.7%), while simultaneously extend lifespan 30% in 16-month-old C57BL/6J male mice⁵⁴. These disparities in lifespan outcomes between the two studies are likely attributed to the age of the mice. In another study¹¹, the Geometric Framework was employed to design 30 different diets with varying proportions of cellulose, protein, carbohydrates, and fats, while maintaining similar levels of other ingredients. This experimental approach was used to assess the impact of macronutrients on longevity in 3-week-old C57BL/6 mice under AL conditions. Intriguingly, diets closely resembling the CF30m diet exhibited significantly longer lifespans compared to the others. Therefore, this unique diet shows promising potential for promoting longevity, suggesting that substituting ~30% of macronutrients with indigestible cellulose may represent an optimal formula for designing caloric restriction mimetics. It's important to note that exceeding 30% cellulose might lead to malnutrition, while falling below this threshold could produce insignificant effects.

The fiber modification could provide a novel approach for nutrient optimization. Numerous evidence demonstrated that high-fiber diets not only benefit gut microbiota but also offer various advantages to the human body, including weight management, reduced hunger, prolonged satiety, immune system homeostasis, inflammation suppression, and decreased risk of several chronic diseases^{13,14,55}. In our study, we designed and tested several high-fiber diets in C57BL/6J male mice. These diets induced significant effects on food, calories, protein or carbohydrate consumption, and body weight gain. Surprisingly, only one diet resulted in a robust systemic response associated with the anti-aging effects typically observed with CR. This finding aligns with previous studies showing that not only the fiber amount but also the fiber source had a crucial impact on nutrient optimization^{15,56}.

We implemented a modified approach involving a circadian-aligned, unrestricted feeding regimen in young mice, differing from the traditional CR method, which typically uses a fixed daily food allotment to control food intake²². Notably, our protocol eliminates the need for precise daily food preparation. In our experiment, the animals were provided with a 2 h feeding window in the evening, from 6 to 8 pm. They appeared to eat normally and consistently achieved ~80% of AL food intake levels. This resulted in ~20% reduction in body weight, indicating the successful establishment of a circadian-aligned 20% CR regimen, a similar protocol to which has been shown to achieve a 35% lifespan extension in male C57BL/6J mice²⁰. Notably, mice fed under this regimen exhibited hepatic transcriptomic and metabolomic profiles and healthy aging signatures similar to those commonly observed in the CR animals.

The nighttime 4-h refeeding protocol exhibited promising potential for investigating the impact of nutrients on hepatic multi-omics profiles in mice. In this study, we chose the 4-h timepoint (10 pm) after a 20 h fasting and refeeding period (6 pm to 10 pm) for profiling multi-omics. This duration is sufficient to induce significant changes in gene expression and metabolites in

both human cells and mouse tissues^{57–59}. Additionally, this specific time window minimizes potential impacts from subsequent meals (akin to human lunch), as the refeeding regimen emulates the human breakfast pattern. Establishing a standardized sampling condition is crucial for investigating the effects of nutrients on gene expression and metabolism, given the significant influence of biological rhythms and environmental factors. For example, in mouse circadian rhythm studies, increasing sampling frequency (e.g., collecting samples every 2 or 4 h over a 24 h period) can help reduce potential sources of noise^{20,35}. However, implementing such protocols in clinical settings may present challenges.

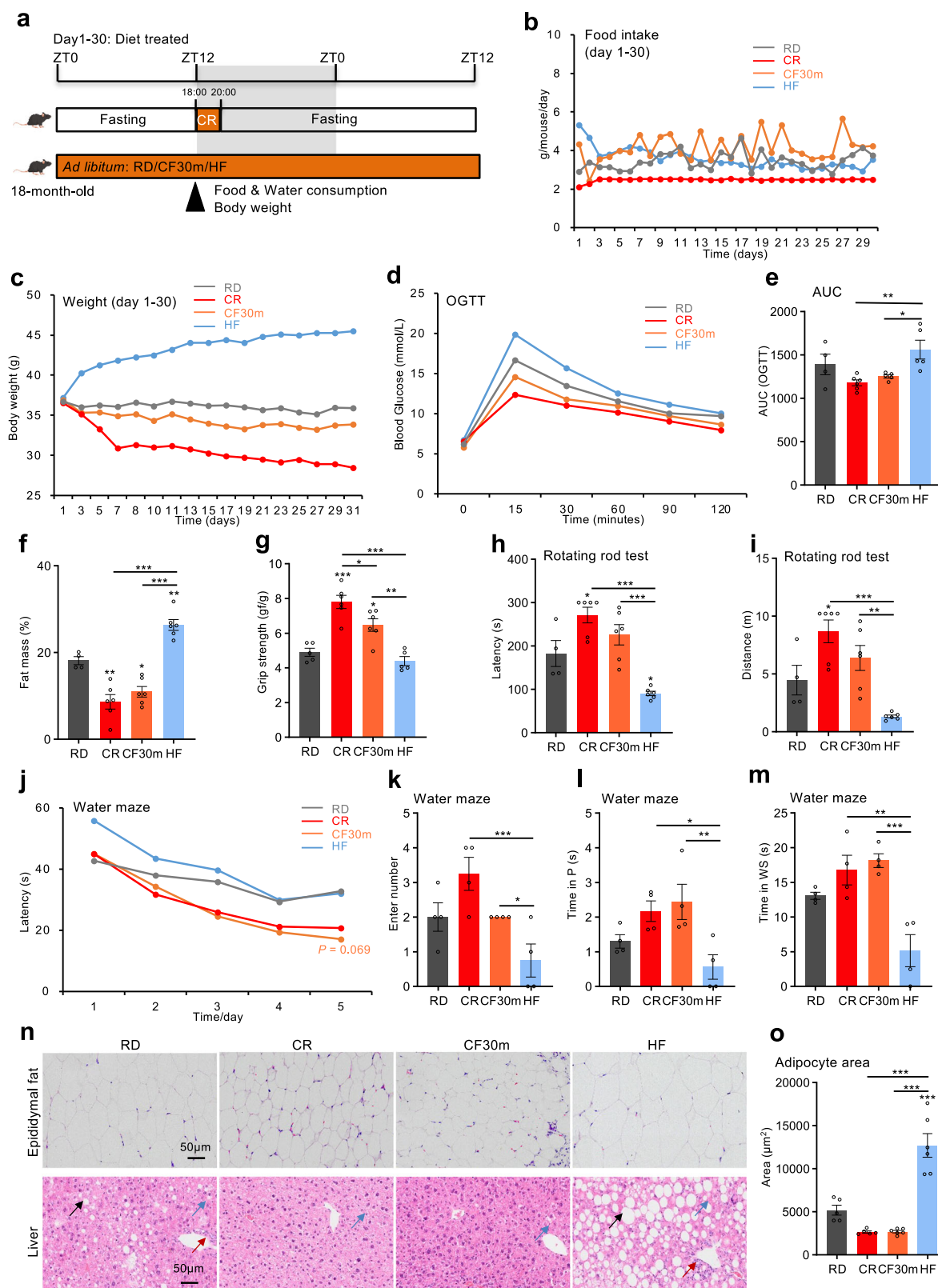
The findings presented here are primarily observational, providing a robust foundation for understanding the phenotypic parallels between high-fiber diets and CR. However, the precise molecular mechanisms underlying these effects remain to be fully elucidated. Specifically, we measured SCFAs and ketone body levels to explore potential pathways, such as those involving G protein-coupled receptors (e.g., GPR43) or histone deacetylase (HDAC) inhibition, which are well-established in dietary fiber research⁴². Although SCFAs and ketone levels showed minimal changes under the CF30m diet compared to CR, consistent with prior studies, we did not perform direct mechanistic experiments, such as SCFA supplementation or the use of receptor knockout models, to test these pathways explicitly. This limitation constrains our ability to draw definitive mechanistic conclusions at this stage. The observed benefits of the CF30m diet—improved glucose and lipid metabolism, enhanced motor and cognitive function, and delayed aging markers—may involve complex interactions beyond SCFAs, potentially including gut microbiota dynamics, bile acid metabolism, or other signaling pathways⁴¹. These possibilities warrant further investigation. Additionally, while our study controlled for circadian timing and caloric content to ensure rigorous comparisons, extending these findings to other dietary fiber types or mammalian species could further validate the generalizability of the CF30m diet's effects.

In summary, although the mechanisms underlying the effectiveness of this high-fiber diet remain unclear, our integrative analysis of feeding behaviors, growth, and aging-related markers⁶⁰ in male mice from young to old age demonstrates that the CF30m diet can replicate the health benefits of the circadian-aligned CR. These benefits include unrestricted food intake without hindering body weight gain, improved glucose metabolism, reduced body fat, enhanced motor and cognitive function, and geroprotective effects observed at the transcriptomic and metabolomic levels. Consequently, this diet emerges as a promising candidate for further exploration of CR-like benefits on health and aging.

Methods

Diets

Based on the AIN-93G standard mouse diet, we designed eight specialized dietary fiber diets: 10% Inulin / Cellulose Fiber Diet (IF10/CF10), 20% Inulin / Cellulose Fiber Diet (IF20/CF20), 30% Inulin / Cellulose Fiber Diet (IF30/CF30), and 30% Inulin / Cellulose Fiber Diet modified (IF30m/CF30m). All fiber diets and a high fat diet (D09100310) were



customed from Xietong Pharmaceutical Bio-engineering Co., Ltd (Jiangsu, China). The IF10/CF10, IF20/CF20, and IF30/CF30 sets were formulated by replacing an equivalent amount of corn starch in the AIN-93G diet, while IF30m/CF30m sets adjusted the macronutrient content to 70% of the AIN-93G diet and supplemented it with 30% inulin or cellulose dietary fiber. All fiber contents in the diets were verified as available.

Animal and experimental details

This study was performed in accordance with the recommendations in the Guide for the Care and Use of Laboratory Animals and relevant Chinese laws and regulations. All procedures involving mice and experimental protocols were approved by the Institutional Animal Care and Use Committee (IACUC) of Shanghai Jiao Tong University (Animal Protocol No. A2020042). Healthy C57BL/6J male mice were

Fig. 7 | A high-fiber diet improves physical performance in naturally aging mice. **a** Outline of feeding regimens (RD, CR, HF and CF30m) over 30 days. Food and water consumption were measured at ZT12. **b** Body weight changes over 30 days. **c** Average food intake of all groups during the 30 days. **d** Blood glucose levels after oral glucose gavage over 120 min. **e** AUC of glucose levels in all groups during the 120-min OGTT. For RD group, $n = 4$ mice; For HF and CF30m group, $n = 5$ mice; For CR group, $n = 6$ mice. **f** Fat mass comparison from body composition analysis. For RD group, $n = 4$ mice; For HF, CF30m and CR group, $n = 6$ mice. **g** Grip strength comparison. For RD and HF group, $n = 5$ mice; For CF30m and CR group, $n = 6$ mice. **h, i** Latency time (**g**) and movement distance (**h**) in rotating rod test. For RD group,

$n = 4$ mice; For HF, CF30m and CR group, $n = 6$ mice. **j** Escape latency in the Morris water maze test. Morris water maze measures: target platform enter number (**k**), crossing time (**l**), and WS quadrant crossing time (**m**). $n = 4$ mice per group. Histological analysis of epididymal fat and liver sections stained with H&E (**n**). Individual adipocyte areas in epididymal fat sections were analyzed (**o**). In liver sections, black arrowheads indicate lipid droplets, red arrowheads indicate inflammatory cell infiltration, and blue arrowheads indicate edematous liver cells. For RD group, $n = 5$ mice; For CF30m, HF and CR group, $n = 6$ mice. Data are presented as mean \pm SEM. Statistical significance was determined by one-way ANOVA (Tukey post-hoc test). * $P < 0.05$, ** $P < 0.01$, *** $P < 0.001$.

purchased from Vital River, Inc (Zhejiang, China). All mice were group housed at 5–6 mice per cage in Experimental Animal Center, Shanghai Jiao Tong University, with a 12 h light: 12 h dark cycle, at a temperature of 18–23 °C, and 50 \pm 2% humidity.

Seven-week-old C57BL/6J male mice ($n = 60$) underwent a 20 h fasting period (with free access to water) after a one-week acclimatization feeding. The animals were then divided into eight fiber diet groups, one AIN-93G regular diet (RD) group, and one calorie restriction (CR) group. After switching to the customized diet ad libitum, food and water intake were measured hourly over the next 4 h (from 18:00 to 22:00). Over the following 13 days, the CR group was fed the AIN-93G diet but was restricted to eating only during the most active 2 h period (18:00–20:00) of the circadian rhythm, while the other 9 groups were fed ad libitum. Water was provided ad libitum throughout the study. Food intake, water intake, and body weight were measured daily at 18:00. On Day 13 and 14, the same fasting and 4-h intake test protocol as on Day 0 and 1 was repeated. All mice were sacrificed by rapid cervical dislocation, and hepatectomy was performed.

To confirm the positive effects of the high-fiber diet (CF30m) on delaying aging, dietary interventions were conducted on middle-aged and naturally aging mice. After a 4-month acclimatization period, 6-month-old animals ($n = 10$) were divided into two diet groups: one AIN-93G regular diet (RD) group and one high fiber diet (CF30m) group, both with ad libitum access to water and food. Food intake, water intake, and body weight were measured every 5 days until all mice were sacrificed. At week 12, 8-week-old young C57BL/6J male mice ($n = 6$) were purchased. Grip strength, Y Maze, rotating rod, Morris water maze and oral glucose tolerance tests (OGTT) were assessed during week 14 and week 15.

After an 8-month acclimatization period, 18-month-old mice underwent a 20 h fasting period (with free access to water). The animals were divided into four diet groups, RD, CR, CF30m and high fat (HF) diet groups. The CR group was fed the AIN-93G diet but was restricted to eating only 70% of the RD group's intake during the most active 2 h period (18:00–20:00) of the circadian rhythm, while the other three groups were fed ad libitum. Water was provided ad libitum throughout the study. Food intake, water intake, and body weight were measured daily at 18:00 over 30 days. The same fasting and 4 h intake test protocol as on Day 0 and 1 was repeated before all mice were sacrificed. The grip strength, body composition, rotating rod, Morris water maze and OGTT were conducted during week 4.

Collection of tissue

The CR group was allowed to eat from 18:00 to 20:00 as usual, the other groups were allowed to eat their diets ad libitum for 4 h following a 20 h fasting period. Autopsies were performed at 22:00. One animal was randomly dissected per group until all dissections were completed.

Histological analysis

Tissues were fixed in 4% paraformaldehyde in PBS and stored in 70% ethanol. Fixed tissues were embedded in paraffin using standard

procedures. Tissue blocks were sectioned (5 μ m) and stained with hematoxylin and eosin (H&E). Adipocyte size was quantitatively evaluated using Image J by manually outlining five randomly selected adipocytes per section. Skin samples (1 cm²) were collected from the telogen hind backskin (0.5–1 cm away from the tail), and subdermal thicknesses were measured. At least 10 measurements were taken from each replicate, and mean values were calculated. Regions with low structural integrity were excluded from analysis.

RNA extraction

Approximately 10 mg of liver tissue (left lobe) was immersed in 600 μ l TRIzol, homogenized thoroughly, snap-frozen in liquid nitrogen, and stored at -80 °C for RNA extraction the following day. All samples were ground using a high throughput tissue grinder at 300 g for 30 s (repeated three times). Following centrifugation at 14,000 g at 4 °C for 10 min. RNA was extracted using M5 HiPer Universal Plus RNA Mini Kit (Mei5 Biotech, Beijing, China) according to manufacturer instructions. All RNA samples used had a RIN > 8.

RNA sequencing

All RNA samples were sent to Novogene Co., Ltd (Beijing, China) for quality control (Sample QC). After RNA library preparation, cDNA libraries are sequenced on Illumina NovaSeq platforms using a paired-end 150 bp sequencing strategy. Approximately 6 G clean data and a >75% uniquely mapped reads rate for each sample were obtained for each sample. Six biological replicates were included.

Processing and analysis of RNA-Seq data

FASTQ output files were aligned to *Mus musculus* GRCh39 reference genomes using STAR with a 2-pass procedure. Genes and transcripts (Aligned.sortedByCoord.out.bam file from STAR outputs) were quantified using RSEM. Differential expression analysis of genes and transcripts was performed in R using the Bioconductor package DESeq2. A threshold of FDR (padj) < 0.05 was set to determine differentially expressed genes (Supplementary Data 1, 5, 6).

GO term and pathway annotation

GO biological process and KEGG pathway enrichment analyses were performed using David (version 2021). Heatmaps were generated from the counts using Morpheus (<https://software.broadinstitute.org/morpheus>). Genes network graphs were created using STRING.

Gene Set Enrichment Analysis (GSEA)

GSEA v2.2.0 was used for pathway enrichment analysis. Weighted enrichment scores were calculated with gene expression lists ranked by signal-to-noise ratio (maximum gene set size: 500; minimum gene set size: 20; number of permutations: 1000; gene set database: Hallmark; false discovery rate [FDR] < 0.25; and $P < 0.01$).

DR-regulated genes in young and old mice

In this study, we re-analyzed the gene expression datasets (GSE190939) collected by Acosta-Rodriguez et al. using the same method described above (Supplementary Data 2, 3).

Metabolite extraction

The metabolite extract was a mixture of methanol/acetonitrile/water (2:2:1, v/v/v), with an internal standard (2.0 µg/mL, DL-*o*-chlorophenylalanine) added. A total of 300 µL of cold metabolite extract was added to 50 mg of liver tissue, followed by homogenization using metal beads in a high throughput tissue grinder at 300 g for 30 s, repeated three times. After vortexing, samples were incubated at -20 °C for 60 min and then centrifuged at 12,000 *g* for 10 min at 4 °C. The supernatants were transferred to a new tube. An additional 200 µL of metabolite extract was added to the pellet, vortexed, incubated at -20 °C for 30 min, and centrifuged again. The resulting supernatant was combined with the initial supernatant, centrifuged once more, and dried in a vacuum concentrator. Finally, the dried metabolite extracts were reconstituted with 100 µL methanol/water (3:7, v/v), vortexed, centrifuged at 14,000 *g* for 20 min at 4 °C, and 40 µL of the supernatant was transferred to an injection vial for analysis. Quality control (QC) samples were prepared by mixing 5 µL of the extracts of all samples.

Untargeted metabolomics

For the liver untargeted metabolomic, there were a total of 32 samples. There were 5 biological replicates for the RD, IF30, IF30m, and CF30 groups, and 6 biological replicates for the CR and CF30m groups. Quality control (QC) samples were prepared by pooling 5 µL aliquots from each experimental sample and were injected every three samples to monitor the stability of the analytical system.

Before analysis, three QC samples were injected to equilibrate the analytical system. During analysis, a QC sample was injected after every three sample injections to evaluate system stability. Chromatographic conditions were as follows: A Vanquish UHPLC/Q Exactive plus system (ThermoFisher) equipped with an ACQUITY UPLC HSS T3 (100 × 2.1 mm, 1.7 µm, Waters Co., US) was used for untargeted metabolomic analysis. The column temperature was maintained at 40 °C, and the injection volume was 1 µL per sample. The gradient mobile phase consisted of 0.1% formic acid in water (A) and 0.1% formic acid in acetonitrile (B). The flow rate was 0.4 mL/min, with the gradient set as follows: A/B 99/1–0/100 over 12 min, hold in 0/100 from 12–13 min. Mass spectrometric conditions were as follows: Ionization was performed in both positive and negative heated electrospray ionization (H-ESI) modes, with scanning mode based on Data Dependent Acquisition (DDA). One full scan was followed by 10 MS/MS scans. The collision energy was set to NEC15,30 for ion fragmentation, and nitrogen (99.999%) was used as the collision-induced dissociation gas. The scan range was 67–1000 amu. Full scan parameters included a resolution of 70,000, AGC of 1e⁶, and IT of 100 ms. Secondary mass spectrum Settings included dd-MS/MS resolution of 17,500, AGC of 5e⁵, IT of 50 ms. Spray voltages were 3.2 kV (positive mode) and 2.8 kV (negative mode), with a capillary temperature of 320 °C and an s-lens RF level of 50 V.

Mass spectrometry data analysis

Data acquisition was performed using Xcalibur 3.0 software (ThermoFisher). The raw data were imported into Progenesis Q1 v2.3 software (Waters Co., USA) for peak alignment, peak picking, and deconvolution. Metabolites were identified by comparing information from online databases (Human Metabolome database: <https://www.hmdb.ca/>, LIPID MAPS: <https://www.lipidmaps.org/>, and MS/MS spectral databases Metlin: <https://metlin.scripps.edu/>). Differential metabolites were selected when the FC > 1.50 and the *P* value < 0.05 (Supplementary Data 4). All differential metabolites were analyzed using IMPaLA (<http://impala.molgen.mpg.de/>) for pathway over-representation analysis.

Joint pathway analysis

Integrative analysis of transcriptomics and metabolomics data for pathway over-representation analysis was performed using IMPaLA (<http://impala.molgen.mpg.de/>).

Targeted fatty acid quantitation

For short-chain fatty acid targeted mass spectrometry, there were 34 samples in total, 17 serum samples and 17 liver samples. There were 6 biological replicates in the RD and CF30m groups, and 5 biological replicates in the CR group.

For serum samples, 100 µL of serum was sequentially mixed with 75 µL of 50% H₂SO₄ and 300 µL of methyl tert-butyl ether (MTBE) solution containing 0.4 µg/mL 2-methylpentanoic acid (internal standard). The mixture was vortexed for 1 min, centrifuged at 14,000 *g* for 20 min, and incubated at 4 °C for 30 min. The resulting supernatant was collected for GC-MS analysis. For liver tissue, 0.2 g of tissue was homogenized with 50 µL of sterile water using bead grinding, followed by the addition of 50 µL of 50% H₂SO₄ and 200 µL of MTBE containing 0.4 µg/mL 2-methylpentanoic acid. The mixture was vortexed for 1 min, centrifuged at 14,000 *g* for 10 min, and incubated at 4 °C for 30 min. The supernatant was subsequently collected for GC-MS analysis. Quantification of SCFAs was performed using a GC-MS-7000D system (Agilent Technologies, USA) equipped with a HP-FFAP capillary column (30 m × 0.25 mm, 0.25 µm). Helium (99.999%) was used as the carrier gas with a constant flow rate. One microliter of extract was injected in split mode (split ratio 5:1) with an injector temperature of 250 °C. GC oven temperature program was set as follows: the initial temperature was 100 °C and held for 1 min, followed by a ramp of 5 °C/min to 145 °C, and then a ramp of 40 °C/min to 240 °C, which was held for 8 min. Mass spectrometry was operated in electron impact (EI) mode with a solvent delay of 4 min. Full-scan spectra were acquired in the *m/z* range of 33–350. Selected Ion Monitoring (SIM) was performed in five-time segments: *m/z* 60 from 4.00 to 5.80 min, *m/z* 73 from 5.80 to 7.40 min, *m/z* 60 from 7.40 to 10.05 min, *m/z* 74 from 10.05 to 10.80 min, and *m/z* 60 after 10.80 min.

A series of standard solutions for short-chain fatty acids (SCFAs), including Acetic acid, Propionic acid, Isobutyric acid, Butyric acid, Isovaleric acid, Valeric acid, and Caproic acid, were prepared at the following concentrations: 2.5 ng/mL, 5 ng/mL, 10 ng/mL, 25 ng/mL, 50 ng/mL, 100 ng/mL, 200 ng/mL, 400 ng/mL, 800 ng/mL, 1000 ng/mL, 2500 ng/mL, 5000 ng/mL, and 10000 ng/mL. These standards were used for calibration and the construction of the calibration curve for the GC-MS analysis of SCFAs in serum and liver samples.

Raw data acquisition was performed using MassHunter Workstation software (Build 12.1.938.3). Peak identification and quantification were based on retention time and characteristic ion fragments, using external calibration curves of authentic SCFA standards. Data processing and integration were performed with MassHunter Quantitative Analysis software.

Y Maze

The Y maze task was performed to assess spontaneous alternation, defined as successive entries into the three arms in overlapping triplet sets. The maze includes three arms converging at equal angles. Each arm measures 35 cm in length, 5 cm in width, and 10 cm in height. The mouse was placed at the end of one arm, numbered as 1, with the other two arms numbered as 2 and 3. The mouse was allowed to explore for 8 min, during which the total number of arm entries, alternations, and exploration time were recorded. The percentage of correct alternation was calculated as the ratio of actual to total alternations, defined as (the total number of arm entries – 2) × 100%.

Grip strength test

The strength of all four limbs of mice was measured using the grip strength test according to the manufacturer's instructions. Mice were placed on the grid with all four paws attached and gently pulled back to measure grip strength until the grid was released. The values obtained represent the muscle force (gf) obtained in *n* = 3 trials per animal, with a 5 min interval between trials, normalized to the respective body weight (g).

Aging parameter evaluation

At the end of the observation period, mice were assessed for typical aging signs. A scoring system was used to evaluate animal status, ranging from 0 to 3 for fur condition, where 0 indicates no gray fur and 3 indicates extensive gray fur.

Rotating rod test

The rotating rod instrument consists of six channels, each equipped with a rotating rod. When a mouse fell from the rod, the machine stopped and recorded the time of fall and the corresponding distance traveled. Following a previously established method, mice underwent three daily training sessions for three days, and the fourth day was designated as the official testing day. The rotating rod started at a speed of 4 rpm and gradually increased to a maximum of 40 rpm within 300 s. If a mouse fell within the first 30 s of a test, it was considered an accidental slip, and the test was repeated.

Morris water maze

The Morris water maze was used to evaluate spatial memory acquisition over five days of trials. A circular pool with a diameter of 160 cm and a depth of 50 cm was prepared, divided into four quadrants, and filled with white pigment to create a contrasting background. Drapes were used to obscure the mouse's surroundings, and high-contrast spatial cues were placed inside the pool. The escape platform, a cylindrical structure, was located in the WS quadrant. A behavior detection system connected to a camera and computer was used to track the mice. On Day 1, a visible platform trial was conducted to confirm that the mice could swim and had normal vision, with the platform set 1 cm above the water surface. Days 2 to 5 involved hidden platform trials, where the platform was submerged 1 cm below the surface. If a mouse reached the platform within 60 s and remained for 5 s, the computer recorded the escape latency. If unsuccessful, the mouse was placed on the platform for 20 s, and the escape latency was recorded as 60 s. On Day 6, during the spatial probe test, the platform was removed, and the number of platform crossings and movement routes within 60 s were recorded.

Body composition

The body composition of all mice was measured using a body composition analyzer according to the manufacturer's instructions.

Oral glucose tolerance test

An oral glucose tolerance test (OGTT) was performed prior to the Morris water maze test but after other behavioral experiments. Mice were fasted for 12 h before receiving a glucose bolus (2 g/kg). Fasting blood glucose was measured prior to administration, and blood glucose levels were recorded at 15, 30, 45, 60, 90, and 120 min post-administration by clipping the tails and using a glucometer from Sinocare inc. (Hunan, China). Mice were re-fed after the final blood sample was collected.

Blood ketone measurement

At 18:00 and 22:00, blood ketone (β -hydroxybutyrate) levels were measured in blood samples collected from the tip of the tail vein with a blood ketone meter from Sinocare inc. (Hunan, China).

Statistical analysis

Differences among means were analyzed using one-way ANOVA for multiple comparisons. When ANOVA analysis revealed significant differences, pair-wise comparisons were performed using Dunnett's test or Tukey post-hoc test as indicated. Unless otherwise stated, all values are presented as mean \pm SEM with statistical results presented as: * $P < 0.05$, ** $P < 0.01$, and *** $P < 0.001$. Spearman correlations were used to evaluate dependencies between two variables (non-parametric, without assuming normal distribution).

Reporting summary

Further information on research design is available in the Nature Portfolio Reporting Summary linked to this article.

Data availability

The RNA-seq raw sequencing data generated in this study have been deposited in the Gene Expression Omnibus (GEO) under the data identifier [GSE296874](https://doi.org/10.1038/s41467-025-61046-z). The mass spectrometry-based untargeted metabolomics data have been deposited in the Metabolights under the accession number [MTBLS12479](https://doi.org/10.1038/s41467-025-61046-z). All data are available in the main text or in Supplementary Data 1–6 as indicated. Any other data not presented in the article will be readily provided by request. Source data are provided in this paper. Source data are provided with this paper.

References

- Green, C. L., Lamming, D. W. & Fontana, L. Molecular mechanisms of dietary restriction promoting health and longevity. *Nat. Rev. Mol. Cell Bio* **23**, 56–73 (2022).
- Longo, V. D. & Anderson, R. M. Nutrition, longevity and disease: From molecular mechanisms to interventions. *Cell* **185**, 1455–1470 (2022).
- Lee, M. B., Hill, C. M., Bitto, A. & Kaeberlein, M. Antiaging diets: separating fact from fiction. *Science* **374**, eabe7365 (2021).
- Mair, W. & Dillin, A. Aging and survival: the genetics of life span extension by dietary restriction. *Annu Rev. Biochem* **77**, 727–754 (2008).
- Mihaylova, M. M. et al. When a calorie is not just a calorie: diet quality and timing as mediators of metabolism and healthy aging. *Cell Metab.* **35**, 1114–1131 (2023).
- Madeo, F., Carmona-Gutierrez, D., Hofer, S. J. & Kroemer, G. Caloric restriction mimetics against age-associated disease: targets, mechanisms, and therapeutic potential. *Cell Metab.* **29**, 592–610 (2019).
- Partridge, L., Fuentealba, M. & Kennedy, B. K. The quest to slow ageing through drug discovery. *Nat. Rev. Drug Discov.* **19**, 513–532 (2020).
- Harrison, D. E. et al. Rapamycin fed late in life extends lifespan in genetically heterogeneous mice. *Nature* **460**, 392–U108 (2009).
- Mannick, J. B. & Lamming, D. W. Targeting the biology of aging with mTOR inhibitors. *Nat. Aging* **3**, 642–660 (2023).
- Johnson, S. C., Rabinovitch, P. S. & Kaeberlein, M. mTOR is a key modulator of ageing and age-related disease. *Nature* **493**, 338–345 (2013).
- Solon-Biet, S. M. et al. The ratio of macronutrients, not caloric intake, dictates cardiometabolic health, aging, and longevity in ad libitum-fed mice. *Cell Metab.* **19**, 418–430 (2014).
- Fontana, L. & Partridge, L. Promoting health and longevity through diet: from model organisms to humans. *Cell* **161**, 106–118 (2015).
- Makki, K., Deehan, E. C., Walter, J. & Backhed, F. The impact of dietary fiber on gut microbiota in host health and disease. *Cell Host Microbe* **23**, 705–715 (2018).
- Gill, S. K., Rossi, M., Bajka, B. & Whelan, K. Dietary fibre in gastrointestinal health and disease. *Nat. Rev. Gastro Hepat.* **18**, 101–116 (2021).
- Zhao, L. P. et al. Gut bacteria selectively promoted by dietary fibers alleviate type 2 diabetes. *Science* **359**, 1151–1156 (2018).
- Hatori, M. et al. Time-restricted feeding without reducing caloric intake prevents metabolic diseases in mice fed a high-fat diet. *Cell Metab.* **15**, 848–860 (2012).
- Chaix, A., Lin, T., Le, H. D., Chang, M. W. & Panda, S. Time-restricted feeding prevents obesity and metabolic syndrome in mice lacking a circadian clock. *Cell Metab.* **29**, 303–319 (2019).
- Mitchell, S. J. et al. Daily fasting improves health and survival in male mice independent of diet composition and calories. *Cell Metab.* **29**, 221–228 (2019).

19. Chaix, A., Zarrinpar, A., Miu, P. & Panda, S. Time-restricted feeding is a preventative and therapeutic intervention against diverse nutritional challenges. *Cell Metab.* **20**, 991–1005 (2014).
20. Acosta-Rodríguez, V. et al. Circadian alignment of early onset caloric restriction promotes longevity in male C57BL/6J mice. *Science* **376**, 1192–1202 (2022).
21. Pak, H. H. et al. Fasting drives the metabolic, molecular and geroprotective effects of a calorie-restricted diet in mice. *Nat. Metab.* **3**, 1327–1341 (2021).
22. Acosta-Rodríguez, V. A., de Groot, M. H. M., Rijo-Ferreira, F., Green, C. B. & Takahashi, J. S. Mice under caloric restriction self-impose a temporal restriction of food intake as revealed by an automated feeder system. *Cell Metab.* **26**, 267–277 (2017).
23. Xie, K. et al. Every-other-day feeding extends lifespan but fails to delay many symptoms of aging in mice. *Nat. Commun.* **8**, 155 (2017).
24. Shaw, P. H., Held, W. A. & Hastie, N. D. The gene family for major urinary proteins - expression in several secretory-tissues of the mouse. *Cell* **32**, 755–761 (1983).
25. Kaur, A. W. et al. Murine pheromone proteins constitute a context-dependent combinatorial code governing multiple social behaviors. *Cell* **157**, 676–688 (2014).
26. Hurst, J. L. et al. Individual recognition in mice mediated by major urinary proteins. *Nature* **414**, 631–634 (2001).
27. Cao, S. X., Dhahbi, J. M., Mote, P. L. & Spindler, S. R. Genomic profiling of short- and long-term caloric restriction effects in the liver of aging mice. *P Natl Acad. Sci. USA* **98**, 10630–10635 (2001).
28. Baur, J. A. et al. Resveratrol improves health and survival of mice on a high-calorie diet. *Nature* **444**, 337–342 (2006).
29. Fontana, L., Partridge, L. & Longo, V. D. Extending healthy life span from yeast to humans. *Science* **328**, 321–326 (2010).
30. Hetz, C. Adapting the proteostasis capacity to sustain brain healthspan. *Cell* **184**, 1545–1560 (2021).
31. Ewald, C. Y., Landis, J. N., Abate, J. P., Murphy, C. T. & Blackwell, T. K. Dauer-independent insulin/IGF-1 signalling implicates collagen remodelling in longevity. *Nature* **519**, 97–101 (2015).
32. Taylor, R. C. & Hetz, C. Mastering organismal aging through the endoplasmic reticulum proteostasis network. *Aging Cell* **19**, e13265 (2020).
33. Kenyon, C. J. The genetics of ageing. *Nature* **467**, 622–622 (2010).
34. Ingram, D. K. & de Cabo, R. Calorie restriction in rodents: Caveats to consider. *Ageing Res Rev.* **39**, 15–28 (2017).
35. Deota, S. et al. Diurnal transcriptome landscape of a multi-tissue response to time-restricted feeding in mammals. *Cell Metab.* **35**, 150–165 (2023).
36. Sato, S. et al. Circadian reprogramming in the liver identifies metabolic pathways of aging. *Cell* **170**, 664–677 (2017).
37. Hahn, O. et al. A nutritional memory effect counteracts the benefits of dietary restriction in old mice. *Nat. Metab.* **1**, 1059–1073 (2019).
38. Wishart, D. S. et al. HMDB 5.0: the human metabolome database for 2022. *Nucleic Acids Res* **50**, D622–D631 (2022).
39. Kamburov, A., Cavill, R., Ebbels, T. M. D., Herwig, R. & Keun, H. C. Integrated pathway-level analysis of transcriptomics and metabolomics data with IMPaLA. *Bioinformatics* **27**, 2917–2918 (2011).
40. Fahy, E. et al. Update of the LIPID MAPS comprehensive classification system for lipids. *J. Lipid Res.* **50**, S9–S14 (2009).
41. Ross, F. C. et al. The interplay between diet and the gut microbiome: implications for health and disease. *Nat. Rev. Microbiol.* **22**, 671–686 (2024).
42. Mann, E. R., Lam, Y. K. & Uhlig, H. H. Short-chain fatty acids: linking diet, the microbiome and immunity. *Nat. Rev. Immunol.* **24**, 577–595 (2024).
43. Puchalska, P. & Crawford, P. A. Multi-dimensional roles of ketone bodies in fuel metabolism, signaling, and therapeutics. *Cell Metab.* **25**, 262–284 (2017).
44. Shimazu, T. et al. Suppression of oxidative stress by β -hydroxybutyrate, an endogenous histone deacetylase inhibitor. *Science* **339**, 211–214 (2013).
45. Oveisgharan, S. et al. The time course of motor and cognitive decline in older adults and their associations with brain pathologies: a multicohort study. *Lancet Health Longev.* **5**, e336–e345 (2024).
46. Liang, A. S. et al. Signaling pathways in hair aging. *Front Cell Dev. Biol.* **11**, 1278278 (2023).
47. Salzer, M. C. et al. Identity noise and adipogenic traits characterize dermal fibroblast aging. *Cell* **175**, 1575–1590 (2018).
48. Vembar, S. S. & Brodsky, J. L. One step at a time: endoplasmic reticulum-associated degradation. *Nat. Rev. Mol. Cell Bio* **9**, 944–957 (2008).
49. Hipp, M. S., Kasturi, P. & Hartl, F. U. The proteostasis network and its decline in ageing. *Nat. Rev. Mol. Cell Bio* **20**, 421–435 (2019).
50. Mishra, A. et al. Fasting-mimicking diet prevents high-fat diet effect on cardiometabolic risk and lifespan. *Nat. Metab.* **3**, 1342–1356 (2021).
51. Liu, X. N. et al. High-fiber diet mitigates maternal obesity-induced cognitive and social dysfunction in the offspring via gut-brain axis. *Cell Metab.* **33**, 923–938 (2021).
52. Nguyen, T. T. & Corvera, S. Adipose tissue as a linchpin of organismal ageing. *Nat. Metab.* **6**, 793–807 (2024).
53. Yamamoto, R. et al. Tissue-specific impacts of aging and genetics on gene expression patterns in humans. *Nat. Commun.* **13**, 5803 (2022).
54. Kokkonen, G. C. & Barrows, C. H. The effect of dietary cellulose on life-span and biochemical variables of male-mice. *Age* **11**, 7–9 (1988).
55. Li, H. T. et al. Resistant starch intake facilitates weight loss in humans by reshaping the gut microbiota. *Nat. Metab.* **6**, 578–597 (2024).
56. Arifuzzaman, M. et al. Inulin fibre promotes microbiota-derived bile acids and type 2 inflammation. *Nature* **611**, 578–584 (2022).
57. Saladin, R. et al. Transient increase in obese gene-expression after food-intake or insulin administration. *Nature* **377**, 527–529 (1995).
58. Leonardson, A. S. et al. The effect of food intake on gene expression in human peripheral blood. *Hum. Mol. Genet* **19**, 159–169 (2010).
59. Greenwell, B. J. et al. Rhythmic food intake drives rhythmic gene expression more potently than the hepatic circadian clock in mice. *Cell Rep.* **27**, 649–657 (2019).
60. Lopez-Otin, C., Blasco, M. A., Partridge, L., Serrano, M. & Kroemer, G. Hallmarks of aging: An expanding universe. *Cell* **186**, 243–278 (2023).

Acknowledgements

We thank Professor T. Keith Blackwell (Harvard Medical School) for helpful proofreading and comments. This work was supported by grants from the National Natural Science Foundation of China to Z.W. (82171550) and X.W. (32172223), the National Key R&D Program of China to Z.W. (2023YFF1104204), the Shanghai Jiao Tong University Medical Engineering Cross Research Fund to L.W. (23×010302236), the startup funding from Shanghai Jiao Tong University to L.W. (23×010502198) and China Postdoctoral Science Foundation to Y.W. (BX20220201). We are grateful to the Instrumental Analysis Center and Laboratory Animal Center of Shanghai Jiao Tong University for instrument support and technical assistance.

Author contributions

Conceptualization: Z.W.; Methodology: F.H., L.Y., X.T., R.H., X.Y., L.W. and Z.W.; Investigation: F.H., L.Y., X.T., R.H., X.Y., L.W., Y.W. and Z.W.; Funding acquisition: X.W. and Z.W.; Project administration: Z.W.; Resources: X.W. and Z.W.; Supervision: X.W. and Z.W.; Writing—original draft: F.H., L.Y., X.T., R.H. and Z.W.; Writing—review and editing: X.W. and Z.W.

Competing interests

The authors declare no competing interests.

Additional information

Supplementary information The online version contains supplementary material available at <https://doi.org/10.1038/s41467-025-61046-z>.

Correspondence and requests for materials should be addressed to Xinlin Wei or Ziyun Wu.

Peer review information *Nature Communications* thanks Alessandro Bitto, Charles Mackay and the other anonymous reviewer(s) for their contribution to the peer review of this work. A peer review file is available.

Reprints and permissions information is available at <http://www.nature.com/reprints>

Publisher's note Springer Nature remains neutral with regard to jurisdictional claims in published maps and institutional affiliations.

Open Access This article is licensed under a Creative Commons Attribution-NonCommercial-NoDerivatives 4.0 International License, which permits any non-commercial use, sharing, distribution and reproduction in any medium or format, as long as you give appropriate credit to the original author(s) and the source, provide a link to the Creative Commons licence, and indicate if you modified the licensed material. You do not have permission under this licence to share adapted material derived from this article or parts of it. The images or other third party material in this article are included in the article's Creative Commons licence, unless indicated otherwise in a credit line to the material. If material is not included in the article's Creative Commons licence and your intended use is not permitted by statutory regulation or exceeds the permitted use, you will need to obtain permission directly from the copyright holder. To view a copy of this licence, visit <http://creativecommons.org/licenses/by-nc-nd/4.0/>.

© The Author(s) 2025